Muscleblind regulates *Drosophila Dscam2* cell-type-specific alternative splicing

Joshua Shing Shun Li[1] **and S Sean Millard**[1,✉]

[1]School of Biomedical Sciences, Faculty of Medicine, The University of Queensland, Brisbane, 4072, Australia.

Alternative splicing of genes increases the number of distinct proteins in a cell. In the brain it is highly prevalent, presumably because proteome diversity is crucial for establishing the complex circuitry between trillions of neurons. To provide individual cells with different repertoires of protein isoforms, however, this process must be regulated. Previously, we found that the mutually exclusive alternative splicing of *Drosophila Dscam2* exon 10A and 10B is tightly regulated and crucial for maintaining axon terminal size, dendritic morphology and synaptic numbers. Here, we show that *Drosophila* muscleblind (mbl), a conserved splicing factor implicated in myotonic dystrophy, controls *Dscam2* alternative splicing. Removing *mbl* from cells that normally express isoform B induces the expression of isoform A and eliminates the expression of B, demonstrating that Mbl represses one alternative exon and selects the other. Mbl mutants exhibit phenotypes that are also observed in flies engineered to express a single isoform. Consistent with these observations, *mbl* expression is cell-type-specific and correlates with the expression of isoform B. Our study demonstrates how cell-type-specific expression of a splicing factor can provide neurons with unique protein isoforms

alternative | splicing | Dscam2 | muscleblind
Correspondence: ***s.millard@uq.edu.au***

Introduction

Alternative splicing occurs in approximately 95% of human genes and generates proteome diversity much needed for brain wiring (Pan et al., 2008; Wang et al., 2008). Specifying neuronal connections through alternative splicing would require regulated expression of isoforms with unique functions in different cell types to carry out distinct processes. Although there are some examples of neuronal cell-type-specific isoform expression (Bell et al., 2004; Iijima et al., 2014; Lah et al., 2014; Norris et al., 2014; Schreiner et al., 2014; Tomioka et al., 2016), the mechanisms underlying these deterministic splicing events remain understudied. This is due, in part, to the technical difficulties of assessing isoform expression at the single cell level. Another obstacle is that most splicing regulators are proposed to be ubiquitously expressed (Nilsen and Graveley, 2010). For example, the broadly expressed SR and heterogeneous nuclear ribonucleoproteins (hnRNPs) typically have opposing activities, and the prevalence of splice site usage is thought to be controlled by their relative abundances within the cell (Blanchette et al., 2009). Although there are many examples where splicing regulators are expressed in a tissue-specific manner (Calarco et al., 2009; Kuroyanagi et al., 2006; Markovtsov et al., 2000; Ohno et al., 2008; Underwood et al., 2005; Warzecha et al., 2009), until recently, reports of cell-type specific expression have been less frequent (McKee et al., 2005; Wang et al., 2018). In insects, Dscam2 is a cell recognition molecule that mediates self- and cell-type-specific avoidance (tiling) (Funada et al., 2007; Millard et al., 2007; Millard et al., 2010). Mutually exclusive alternative splicing of exon 10A or 10B produces two isoforms with biochemically unique extracellular domains that are regulated both spatially and temporally (Funada et al., 2007; Millard et al., 2007). Previously, we demonstrated that cell-type-specific alternative splicing of *Drosophila Dscam2* is crucial for the proper development of axon terminal size, dendrite morphology and synaptic numbers in the fly visual system (Kerwin et al., 2018; Lah et al., 2014; Li et al., 2015). Although these studies showed that disrupting cell-specific *Dscam2* alternative splicing has functional consequences, what regulates this process remained unclear. Here, we conducted an RNAi screen and identified muscleblind (mbl) as a regulator of *Dscam2* alternative splicing. Loss-of-function (LOF) and overexpression (OE) studies suggest that Mbl acts both as a splicing repressor of *Dscam2* exon 10A and as an activator of exon 10B (hereafter *Dscam2.10A* and *Dscam2.10B*). Consistent with this finding, *mbl* expression is cell-type-specific and correlates with the expression of *Dscam2.10B*. Hypomorphic *mbl* mutants exhibit visual system phenotypes that are similar to those observed in flies engineered to express one isoform in all *Dscam2*-positive cells (single isoform strains). Similarly, driving mbl in mushroom body neurons that normally select isoform A, induces the expression of isoform B and generates a single isoform phenotype. Although the mbl gene is itself alternatively spliced, we found that selection of *Dscam2.10B* does not require a specific Mbl isoform and that human MBNL1 can also regulate *Dscam2* alternative splicing. Our study demonstrates that mutually exclusive splicing of *Dscam2* is regulated by the cell-type-specific expression of a highly conserved RNA binding protein, Mbl.

Results

An RNAi screen identifies mbl as a repressor of *Dscam2* exon 10A selection

We reasoned that the neuronal cell-type-specific alternative splicing of *Dscam2* is likely regulated by RNA binding proteins, and that we could identify these regulators by knocking them down in a genetic background containing an isoform reporter. In photoreceptors (R cells) of third instar larvae, *Dscam2.10B* is selected whereas the splicing of *Dscam2.10A*

is repressed (Lah et al., 2014; Tadros et al., 2016). Given that quantifying a reduction in *Dscam2.10B* isoform reporter levels is challenging compared to detecting the appearance of *Dscam2.10A* in cells where it is not normally expressed, we performed a screen for repressors of isoform A in R cells.

To knock down RNA binding proteins, the glass multimer reporter *(GMR)-GAL4* was used to drive RNAi transgenes selectively in R cells. Our genetic background included *UAS-Dcr-2* to increase RNAi efficiency (Dietzl et al., 2007) and *GMR-GFP* to mark the photoreceptors independent of the *Gal4/UAS* system (Brand and Perrimon, 1993). Lastly, a *Dscam2.10A-LexA* reporter driving *LexAOp*-myristolated td-Tomato (hereafter *Dscam2.10A>tdTom*; Fig. 1A) was used to visualize isoform A expression (Lai and Lee, 2006; Tadros et al., 2016). As expected, *Dscam2.10B>tdTom* was detected in R cell projections in the lamina plexus as well as in their cell bodies in the eye-disc, whereas *Dscam2.10A>tdTom* was not (Fig. 1C-1D). Overexpression of Dcr-2 in R cells did not perturb the repression of Dscam2.10A (Fig 1O). We knocked down 160 genes using 250 RNAi lines (Fig 1B and Table S1) and identified two independent RNAi lines targeting *mbl* that caused aberrant expression of *Dscam2.10A* in R cells where it is normally absent (Fig 1F, 1O). The penetrance increased when animals were reared at a more optimal Gal4 temperature of 29°C (Mondal et al., 2007; Ni et al., 2008) (Fig 1O).

Mbl-family proteins possess evolutionarily conserved tandem CCCH zinc-finger domains through which they bind pre-mRNA. Vertebrate Mbl family members are involved in tissue-specific splicing and have been implicated in myotonic dystrophy (Pascual et al., 2006). Formerly known as *mindmelt*, *Drosophila mbl* was first identified in a second chromosome P-element genetic screen for embryonic defects in the peripheral nervous system (Kania et al., 1995). Mbl produces multiple isoforms through alternative splicing (Begemann et al., 1997; Irion, 2012), and its function has been most extensively characterized in fly muscles where both hypomorphic mutations and sequestration of the protein by repeated CUG sequences within an mRNA lead to muscle defects (Artero et al., 1998; Llamusi et al., 2013). To validate the RNAi phenotype, we tested *Dscam2.10A>tdTom* expression in *mbl* loss-of-function (LOF) mutants. Since *mbl* LOF results in lethality, we first conducted complementation tests on six *mbl* mutant alleles to identify viable hypomorphic combinations. These included two alleles created previously via imprecise P-element excision (mbl^{e127} and mbl^{e27}; Begemann et al. 1997) two MiMIC splicing traps ($mbl^{MI00976}$ and $mbl^{MI04093}$; (Venken et al., 2011) and two 2nd chromosome deficiencies (*Df(2R)BSC154* and *Df(2R)Exel6066*; Fig 1F-1G). Consistent with previous reports, the complementation tests confirmed that the majority of the alleles were lethal over one another (Fig 1G) (Kania et al., 1995). However, we identified two *mbl* transheterozygous combinations that were partially viable and crossed these into a *Dscam2.10A>tdTom* reporter background. Both $mbl^{e127}/mbl^{MI00976}$ and $mbl^{MI04093}/mbl^{MI00976}$ animals presented aberrant *Dscam2.10A* expression in R cells when compared to heterozygous and wild-type controls (Fig 1H-O). *Mbl* mutant mosaic clones also exhibited aberrant *Dscam2.10A>tdTom* expression in R cells (Fig S1A-S1F). The weakest allele, mbl^{M00976}, which removes only a proportion of the mbl isoforms, was the only exception (Fig S1E-S1F).

One alternative explanation of how *Dscam2.10A>tdTom* expression could get switched-on in *mbl* mutants, is through exon 10 skipping. Removing both alternative exons simultaneously does not result in a frameshift mutation, and since the Gal4 in our reporters is inserted directly downstream of the variable exons (in exon 11), it would still be expressed. To test this possibility, we amplified *Dscam2* sequences between exon 9 and 11 in $mbl^{e127}/mbl^{MI00976}$ transheterozygous animals using RT-PCR. In both control and *mbl* LOF mutants, we detected RT-PCR products (690bp) that corresponded to the inclusion of exon 10 (A or B) and failed to detect products (390bp) that would result from exon 10 skipping (Fig 1P). This suggested that Mbl is not involved in the splicing fidelity of *Dscam2.10* but rather in the selective mutual exclusion of its two isoforms. To assess whether the ratios of the two isoforms were changing in the mbl hypomorphic mutants, we cut the exon 10 RT-PCR products with the ClaI restriction enzyme that only recognizes exon 10A. Densitometric analysis then allowed us to semi-quantitatively compare the relative levels of both isoforms. There was 25% increase in the level of exon 10A inclusion in $mbl^{e127}/mbl^{MI00976}$ animals compared to controls (Fig 1P). Similarly, qRT-PCR of the $mbl^{e127}/mbl^{MI00976}$ animals showed a 1.25 fold and 0.78 fold change in exon 10A and 10B inclusion respectively, when compared to controls. Both results are consistent with the derepression we observed in our 10A reporter lines. To determine whether Mbl was specifically regulating *Dscam2* exon 10 mutually exclusive splicing, we assessed other *Dscam2* alternative splicing events. These included an alternative 5' splice site selection of *Dscam2* exon 19 and the alternative last exon (ALE) selection of exon 20 (Fig S2A). The expression of these different isoforms was unchanged in *mbl* hypomorphic mutants (Fig S2B). Together, our results indicate that Mbl is an essential splicing factor that specifically represses *Dscam2.10A*.

Mbl is necessary for the selection of *Dscam2* exon 10B

Since *Dscam2* exon 10 isoforms are mutually exclusively spliced, we predicted that selection of exon 10A would lead to the loss of exon 10B selection. To test this, we conducted mosaic analysis with a repressible cell marker (MARCM) (Lee and Luo, 1999) to analyse *Dscam2.10B* expression in *mbl* mutant clones. In late third instar brains, clones homozygous (GFP-positive) for mbl^{e127} and mbl^{e27} exhibited a dramatic reduction in *Dscam2.10B>tdTom* expression in R cell axons projecting to the lamina plexus compared to controls (Fig 2B, C, E). The absence of *Dscam2.10B>tdTom* in *mbl* mutant clones was more striking during pupal stages (Fig 2D), suggesting that perdurance of Mbl could explain the residual signal observed in third instar animals. These results reveal that *mbl* is cell-autonomously required for the selection of the *Dscam2.10B*.

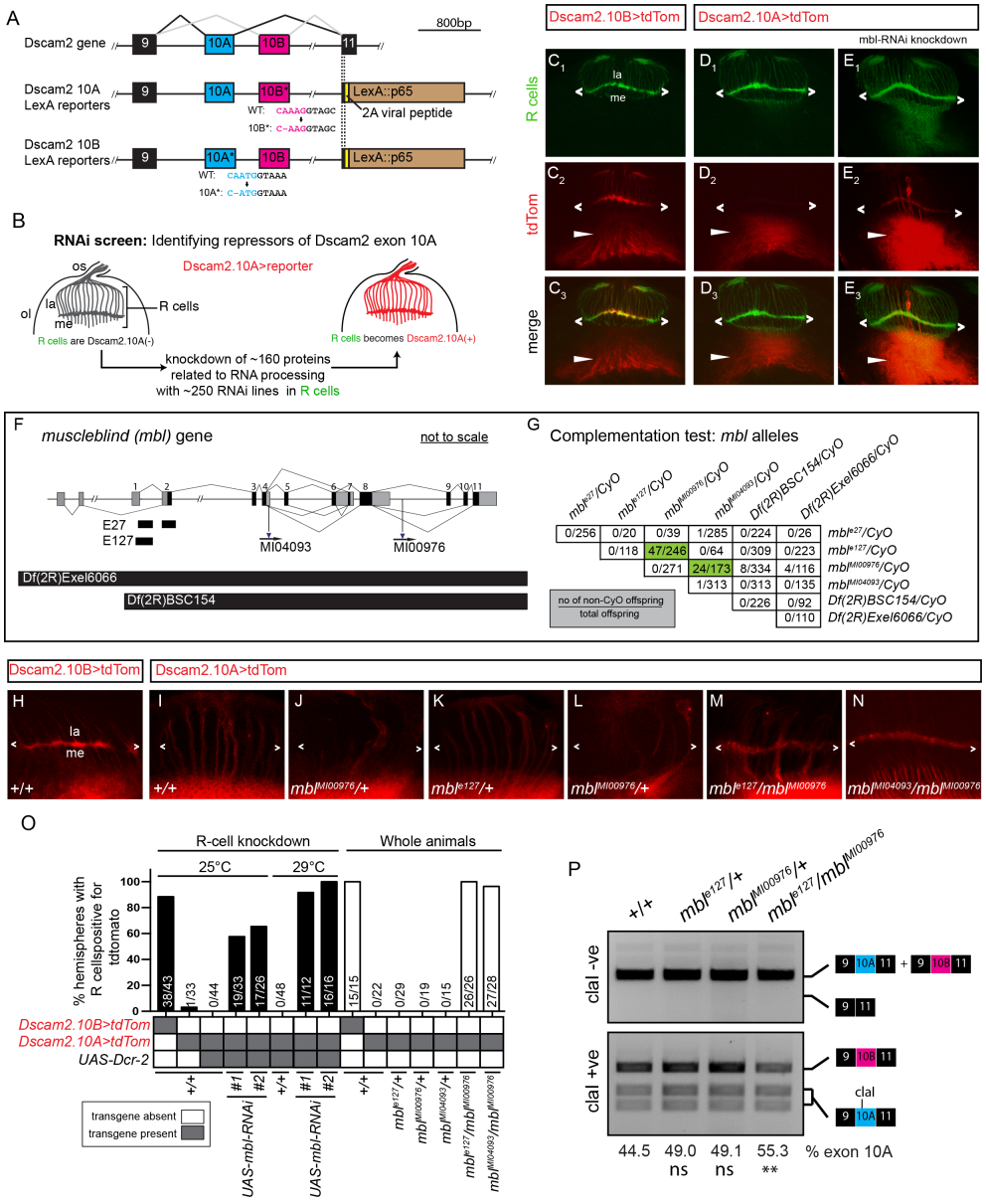

Fig. 1. *Drosophila mbl* is required for the repression of *Dscam2* exon 10A in R cells. (A) Schematic showing the region of *Dscam2* exon 10 that undergoes mutually exclusive alternative splicing and the LexA isoform-specific reporter lines. Frame-shift mutations in the exon not reported are shown. (B) Schematic RNAi screen design for identifying repressors of *Dscam2* exon 10A selection. R cells normally select exon 10B and repress exon 10A. We knocked-down RNA binding proteins in R cells while monitoring 10A expression. (C-E) *Dscam2.10A* is de-repressed in R cells when *mbl* is knocked-down. (C_1-C_3) *Dscam2.10B* control. R cells (green) normally select exon 10B (red). R cell terminals can be observed in the lamina plexus (angle brackets). *Dscam2.10B* is also expressed in the developing optic lobe (arrowhead). (D_1-D_3) *Dscam2.10A* is not expressed in R cells (green) but is expressed in the developing optic lobe (arrowhead). (E_1-E_3) RNAi lines targeting *mbl* in R cells results in the aberrant expression of *Dscam2.10A* in R cells. (F) Schematic of the *mbl* gene showing the location of two small deletions (*e27* and *e127*), two MiMIC insertions (*MI04093* and *MI00976*) and two deficiencies (*Df(2R)Exel6066* and *Df(2R)BSC154*) used in this study. Non-coding exons are in gray, coding exons are black. (G) Complementation test of *mbl* loss-of-function (LOF) alleles. Numbers in the table represent the number of non-CyO offspring over the total. Most transheterygote combinations were lethal with the exception of $mbl^{MI00976}/mbl^{e27}$ and $mbl^{MI00976}/mbl^{MI04093}$ (green). (H-N) Mbl transheterozygotes express *Dscam2.10A* in R cells. (H) *Dscam2.10B* control showing expression in the lamina plexus (angle brackets). (I) *Dscam2.10A* control showing no expression of this isoform in R cells. (J-L) Heterozygous animals for mbl LOF alleles are comparable to control. (M-N) Two different mbl transheterozygote combinations exhibit de-repression of *Dscam2.10A* in R cells. (O) Quantification of *Dscam2.10>tdTom* expression in third instar R cells with various mbl manipulations; including RNAi knockdown (black bars) and whole animal transheterozygotes (white). Y-axis represents the number of optic lobes with R cells positive for tdTom over total quantified as a percentage. On the x-axis, the presence of a transgene is indicated with a grey box and the temperature at which the crosses were reared (25℃ or 29℃) is indicated on the top. (P) *Dscam2.10A* inclusion is increased in mbl transheterozygotes. (Top) Semiquantitative RT-PCR from different genotypes indicated. Primers amplified the variable region that includes exon 10. A smaller product that would result from exon 10 skipping is not observed. (Bottom) Exon 10A-specific cleavage with restriction enzyme ClaI shows an increase in exon 10A inclusion in mbl transheterozygotes. Percentage of exon 10A inclusion was calculated by dividing 10A by 10A+10B bands following restriction digest. The mean of exon 10A inclusion is shown at the bottom of each lane. ANOVA test with Tukey's multiple comparison test was used to compare the exon 10A inclusion. ns $P > 0.05$, ** $P < 0.01$. See also Figures S1 and S2.

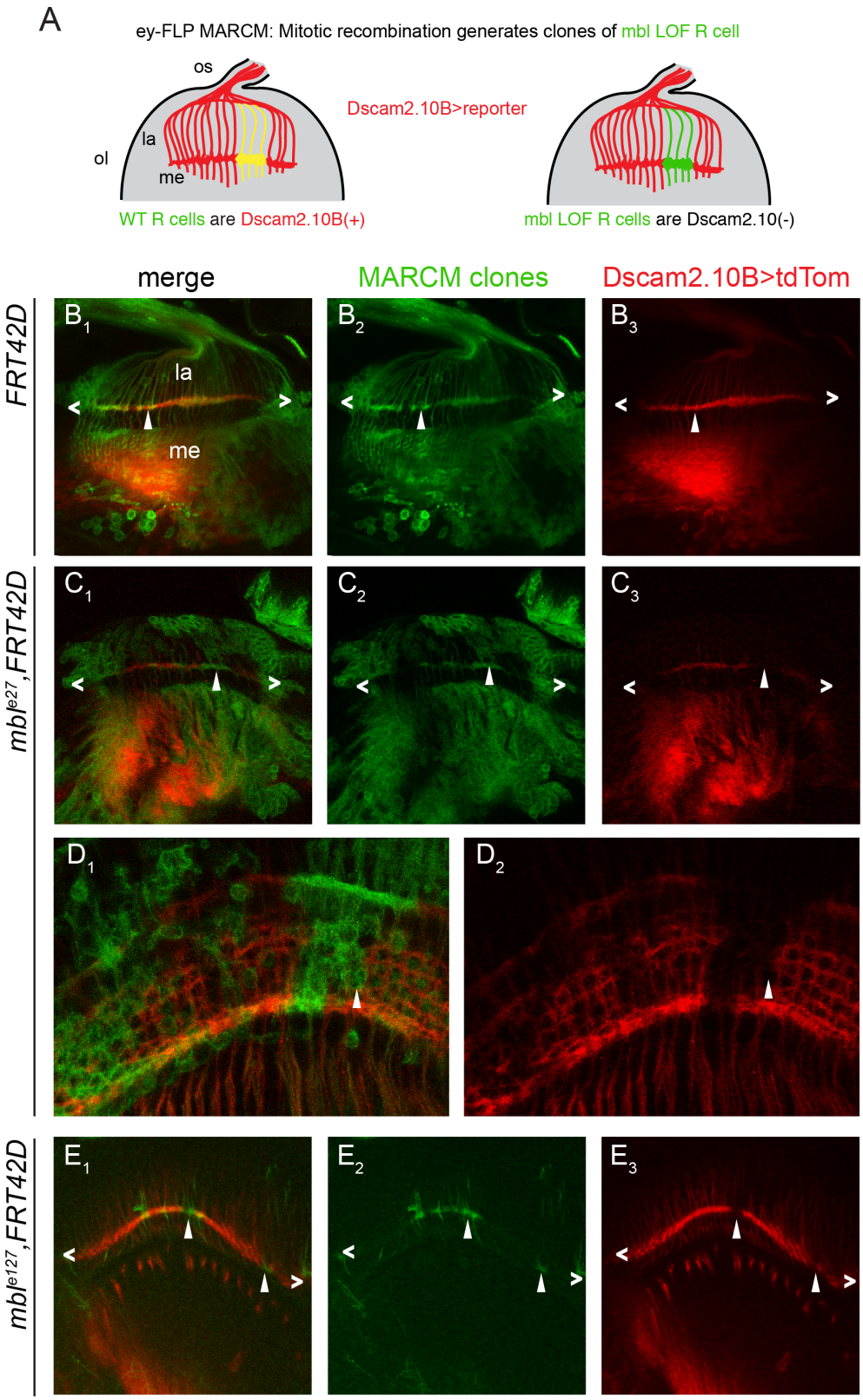

Fig. 2. *Drosophila mbl* is necessary for the selection of *Dscam2* exon 10B in R cells. (A) Schematic of our predicted *mbl* MARCM results using *ey-FLP*. WT R cell clones will be GFP(+) and *Dscam2.10B>tdTom*(+) (yellow), whereas mbl mutant clones will be *Dscam2.10B>tdTom*(-) (green). (B1-B3) Control MARCM clones (green) in 3rd instar R cells (angle brackets) are positive for *Dscam2.10B>tdTom* (arrowhead). (C_1-C_3) In mbl^{e27} clones, *Dscam2.10B* labeling in the lamina plexus is discontinuous and its absence correlates with the loss of *mbl* (arrowhead). (D_1-D_2) *Mbl* MARCM clones from midpupal optic lobes lack *Dscam2.10B>tdTom*. (E_1-E_3) A different allele (mbl^{e127}) exhibits a similar phenotype in third instar brains.

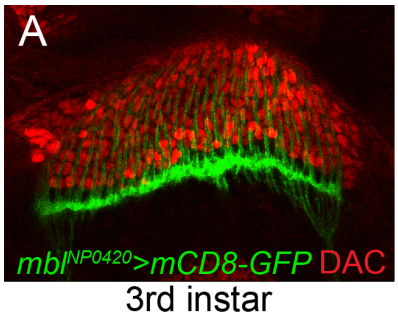

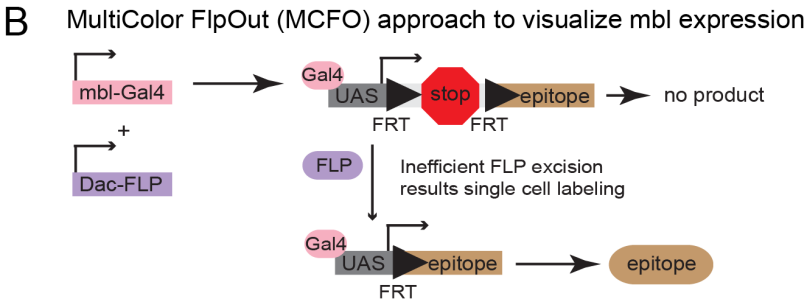

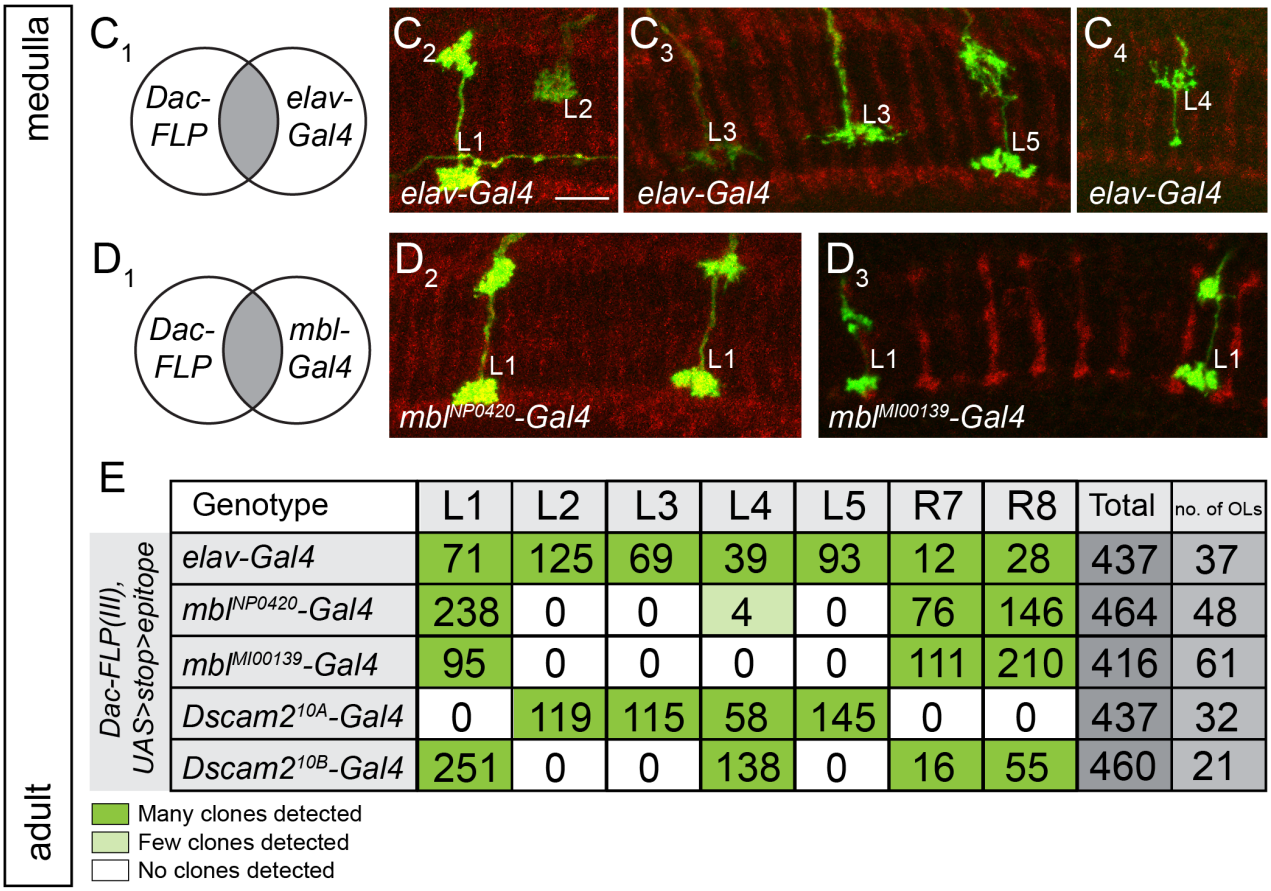

	Genotype	L1	L2	L3	L4	L5	R7	R8	Total	no. of OLs
Dac-FLP(III), UAS>stop>epitope	elav-Gal4	71	125	69	39	93	12	28	437	37
	mblNP0420-Gal4	238	0	0	4	0	76	146	464	48
	mblMI00139-Gal4	95	0	0	0	0	111	210	416	61
	Dscam2 10A-Gal4	0	119	115	58	145	0	0	437	32
	Dscam2 10B-Gal4	251	0	0	138	0	16	55	460	21

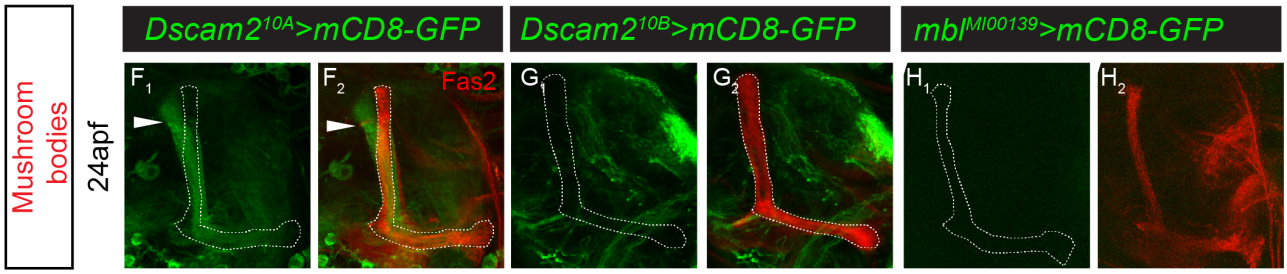

Fig. 3. *mbl* is expressed in a cell-specific manner that correlates with *Dscam2.10B* (A) A *mbl-Gal4* reporter (green) is expressed in third instar R cells but not in lamina neuron precursor cells labeled with an antibody against Dacshund (DAC, red). (B) Schematic of MultiColor FlpOut (MCFO) approach to characterize *mbl* reporter expression in lamina neurons at adult stages. The UAS FlpOut construct produces an epitope-tagged version of a non-fluorescent GFP (smGFP,(Nern et al., 2015)) (C_1-C_4) All lamina neurons can be detected using a MCFO strategy with a pan-neuronal reporter (*elav-Gal4*). Lamina neurons were identified based on their unique axon morphologies. (D_1-D_4) An intersectional strategy using mbl-Gal4 labels primarily L1 lamina neurons. (E) Quantification of lamina neurons and R7-R8 neurons observed using the intersectional strategy. Dark green and light green boxes represent high and low numbers of labeled neurons, respectively. (F-H) *Mbl* is not expressed in mushroom body (MB) neurons that express *Dscam2.10A* at 24hr apf. (F_1-F_2) *Dscam2.10A* is expressed in α'β' MB neurons that are not labeled by Fas2. Fas2 labels the αβ and γ subsets of MB neurons. (G-H) Neither *Dscam2.10B* (G_1-G_2) nor *mbl* (H_1-H_2) are detected in MB neurons. See also Figures S3 and S4.

mbl expression is cell-type-specific and correlates with *Dscam2.10B* selection

Previous studies have reported that Mbl is expressed in third instar eye-discs and muscles (Artero et al., 1998; Brouwer et al., 1997). Since *mbl* LOF results in both the selection of *Dscam2.10A* and the loss of *Dscam2.10B*, we predicted that *mbl* expression would correlate with the presence of isoform B. To test this, we characterized several *mbl* reporters (Fig S3A). We analyzed three enhancer trap strains (transcriptional reporters) inserted near the beginning of the *mbl* gene (mbl^{k01212}-*LacZ*, mbl^{NP1161}-*Gal4* and mbl^{NP0420}-*Gal4*), as well as a splicing trap line generated by the Trojan-mediated conversion of a *mbl MiMIC* (Minos Mediated Integration Cassette) insertion (Fig S2A, $mbl^{Mi00139}$-*Gal4*; (Diao et al., 2015). The splicing trap reporter consists of a splice acceptor site and an in-frame *T2A-Gal4* sequence inserted in an intron between two coding exons. This *Gal4* cassette gets incorporated into *mbl* mRNA during splicing and therefore Gal4 is only present when *mbl* is translated. Consistent with previous studies, and its role in repressing the production of *Dscam2.10A*, all four *mbl* reporters were expressed in the third instar photoreceptors (Fig 3A, S3A-S3D). We next did a more extensive characterization of *mbl* expression by driving nuclear localized GFP (*GFP.nls*) with one transcriptional (mbl^{NP0420}-*Gal4*) and one translational ($mbl^{Mi00139}$-*Gal4*) reporter. In the brain, we found that *mbl* was expressed predominantly in postmitotic neurons with some expression detected in glial cells (Fig SEC-S3H and S3J-S3M). Interestingly, we detected the translational but not the transcriptional reporter in third instar muscles (Fig S3I and S3N). The absence of expression is likely due to the insertion of the P-element into a neural-specific enhancer, as previously described (Bargiela et al., 2014). To assess the expression of *mbl* in the five lamina neurons L1- L5, all of which express *Dscam2* (Lah et al., 2014; Tadros et al., 2016), we implemented an intersectional strategy using a *UAS>stop>epitope* reporter (Nern et al., 2015) that is dependent on both FLP and Gal4. The FLP source (*Dac-FLP*) was expressed in lamina neurons and able to remove the transcriptional stop motif in the reporter transgene. The overlap between *mbl-Gal4* and *Dac-FLP* allowed us to visualize *mbl* expression in lamina neurons at single-cell resolution (Fig 3B). As a proof of principle, we first did an intersectional analysis with a pan-neuronal reporter, *elav-Gal4* (Fig $3C_1$). We detected many clones encompassing various neuronal-cell-types including the axons of L1-L5 and R7-R8 (Fig 3C-3D). This confirmed that all lamina neurons could be detected using this strategy. Using mbl-Gal4 reporters we found that L1, R7 and R8, which expresses *Dscam2.10B*, were the primary neurons labeled. A few L4 cells were also detected, which is consistent with this neuron expressing *Dscam2.10B* early in development and *Dscam2.10A* at later stages (Tadros et al., 2016). To confirm this finding, we dissected the expression of mbl in lamina neurons during development. Using the same intersectional strategy, we detected a high number of L4 clones at 48hr apf (30%, n=10). This was followed by a decline at 60hr apf (26.7%, n = 30) and 72hr apf (11.8%, n = 85) reaching the lowest at eclosion (Fig S4A and S4B;1.7%, n=242). Thus, mbl expression in L4 neurons mirrors the expression of *Dscam2.10B*. Consistent with this, L2, L3 and L5, were all detected using the intersectional strategy with *Dscam2.10A-Gal4* but were not labeled using *mbl-Gal4* (Fig 3E). The expression of *mbl* is further strengthened by an independent RNA-seq study of isolated lamina neurons during development, where *mbl* is detected at high levels in L1, R7 and R8 neurons (~5-100 fold more than L2-L5)(Tan et al., 2015). Together, these results show *mbl* expression correlates with the cell-type-specific alternative splicing of *Dscam2.10B*. Importantly, this suggests that simply the presence or absence of *mbl* can determine the selection of the *Dscam2.10* isoform in a cell.

Ectopic expression of multiple *mbl* isoforms is sufficient to promote the selection of *Dscam2* exon 10B

Since cells that select *Dscam2.10B* express *mbl* and cells that select *Dscam2.10A* lack *mbl*, we wondered whether it was sufficient to promote exon 10B selection in *Dscam2.10A*-positive cells. To test this, we ectopically expressed *mbl* with a ubiquitous driver (*Act5c-Gal4*) and monitored isoform B expression using *Dscam2.10B>tdTom*. We focused on the mushroom body (MB), as this tissue expresses isoform A specifically in α'β' neurons at 24hr apf where *mbl* is not detected (Fig 3G-3H, 4A-4C). Consistent with our prediction, ectopic expression of *mbl* using an enhancer trap containing a UAS insertion at the 5' end of the gene ($Act5c>mbl^{B2\text{-}E1}$), switched on *Dscam2.10B* in α'β' MB neurons, where it is normally absent (Fig 4D). Driving *mbl* with a MB-specific Gal4 (*OK107*) gave similar results (Fig 4E). Although our two Gal4 drivers expressed *mbl* in all MB neurons, *Dscam2.10B* was only observed in α'β' neurons, demonstrating that transcription of *Dscam2* is a pre-requisite for this splicing modulation. Previous studies have suggested that the *mbl* gene is capable of generating different isoforms with unique functions depending on their subcellular localization (Vicente et al., 2007). This also includes the production of a highly abundant circular RNA that can sequester the Mbl protein (Ashwal-Fluss et al., 2014; Houseley et al., 2006). To assess whether *Dscam2* exon 10B selection is dependent on a specific alternative variant of Mbl, we overexpressed the cDNAs of fly *mbl* isoforms (*mblA*, *mblB* and *mblC*; (Begemann et al., 1997; Juni and Yamamoto, 2009) as well as an isoform of the human MBNL1 that lacks the linker region optimal for CUG repeat binding (MBNL135; (Kino et al., 2004; Li et al., 2008) with either *Act5c-Gal4* or *OK107-Gal4*. These constructs all possess the tandem N-terminal CCCH motif that binds to YCGY sequences and lack the ability to produce *mbl* circRNA. In all cases, overexpression resulted in the misexpression of *Dscam2.10B* in α'β' MBs (with the exception *Act5C>mblC*, which resulted in lethality; Fig 4D-4E). Using semi-quantitative RT-PCR from the *Act5C>mbl* flies, we demonstrated that overexpression of *mbl* did not lead to exon 10 skipping and that it increased exon 10B selection by 8-24% (Fig 4F), depending on the *mbl* isoform used. The inability of Mbl to completely in-

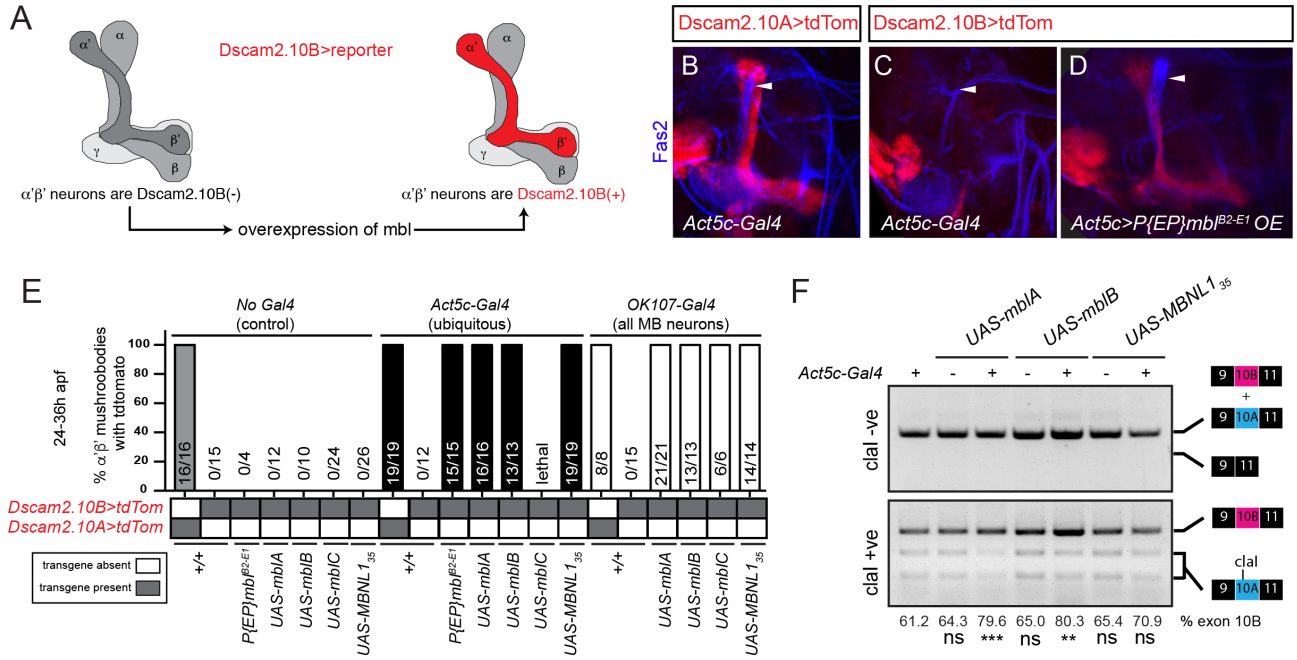

Fig. 4. Multiple *mbl* isoforms promote selection of *Dscam2* exon 10B (A) Schematic showing that *mbl* is sufficient to drive *Dscam2.10B* selection in α'β'neurons. (B) Control showing that *Dscam2.10A* (red) is expressed in α'β' neurons at 24-36hr apf. (C) Control showing that Dscam2.10B is normally repressed in α'β' neurons. (D) Overexpression of mbl activates Dscam2.10B selection (red) in α'β' neurons. (E) Quantification of *Dscam2.10* expression in α'β' neurons at 24-36hr apf with and without mbl OE. Control (No Gal4, grey bar), ubiquitous driver (*Act5c-Gal4*, black bars) and pan-mushroom body neuron driver (*OK107-Gal4*, white bars). Y-axis represents the number of tdTom positive (+) α'β' over the total, expressed as a percentage. Ratio of tdTom(+)/total is shown in each bar. (F) *mbl* OE increases Dscam2 exon 10B inclusion. Semiquantitative RT-PCR as in Figure 1. Exon 10A-specific cleavage with restriction enzyme ClaI shows an increase in exon 10B inclusion in mbl OE animals, without exon 10 skipping. Percentage of exon 10B inclusion was calculated by dividing 10B by 10A+10B bands following electrophoresis and densitometry. The mean of exon 10B inclusion is shown at the bottom of each lane. ANOVA test with Tukey's multiple comparison test was used to compare the exon 10B inclusion. ns $P > 0.05$, ** $P < 0.01$, *** $P < 0.001$.

hibit exon 10A selection suggests that other factors or mechanisms may also contribute to cell-specific *Dscam2* isoform expression (see Discussion). These results suggest that Mbl protein isoforms are all capable of *Dscam2.10B* selection and independent of *mbl* circRNA. The ability of human MBNL1 to promote the selection of exon 10B suggests that the regulatory logic for *Dscam2* splicing is likely conserved in other mutually-exclusive cassettes in higher organisms. Together, our results show that all *mbl* isoforms are sufficient to promote *Dscam2.10B* selection.

Mbl regulates cell-type-specific *Dscam2* alternative splicing in lamina neurons

To determine whether the regulatory logic of *Dscam2* alternative splicing is consistent in other cell types, we manipulated *mbl* expression in lamina neurons (L1-L5). We first asked whether *mbl* LOF resulted in the de-repression of *Dscam2.10A* in L1 neurons. To do this, we visualized *Dscam2* isoform expression in L1-L5 using an intersectional strategy similar to Figure 3 but with a different FLP source (*27G05-FLP*). We detected L1 and L4 neurons when using the *Dscam2.10B-Gal4* reporter in a wild-type background, but not L2, L3 or L5. L1 was also not detected when using the *Dscam2.10A-Gal4* reporter, where L2-L5 cells were the primary neurons labeled (Fig 5A). Consistent with our R cell results, de-repression of *Dscam2.10A* was observed in L1 neurons in *mbl* transheterozygous animals ($mbl^{e127}/mbl^{MI00976}$) when compared to the corresponding heterozygous controls (mbl^{e127}/+ and $mbl^{MI00976}$/+, Fig 5A-5B). We next asked whether ectopic overexpression of *mbl* would result in aberrant *Dscam.10B* selection in L2, L3 and L5 neurons where it is usually repressed. For this experiment, the *Gal4/UAS* system was used to overexpress *mbl* and the *LexA/LexAop* system was used to visualize *Dscam2* isoform expression. Using the same intersectional strategy, we found that *Dscam2-LexA* reporters showed similar patterns to the *Dscam2-Gal4* reporters (Fig 5C). Pan-neuronal overexpression (*elav-Gal4*) of mbl caused the aberrant detection of *Dscam2.10B* in L2, L3 and L5 cells that normally select *Dscam2.10A* (Fig 5C-5D). Together, our results show that Mbl regulates *Dscam2* cell-type-specific alternative splicing. Importantly, the simple presence or absence of *mbl* is sufficient to determine whether a cell expresses *Dscam2.10A* or *Dscam2.10B*.

Manipulation of *mbl* expression generates phenotypes observed in *Dscam2* single isoform mutants

If Mbl regulates *Dscam2* alternative splicing, *mbl* LOF and OE animals should exhibit similar phenotypes to *Dscam2* isoform misexpression. Previously, we showed that flies expressing a single isoform of *Dscam2* exhibit a reduction in L1 axon arbour size and well as reduced dendritic width (Kerwin et al., 2018; Lah et al., 2014). These flies were generated using recombinase-mediated cassette exchange and express a single isoform in all *Dscam2*-positive cells (Lah et al., 2014). The reduction in axonal arbors and dendritic widths were proposed to be due to inappropriate interactions between cells that normally express different isoforms. Consistent with these previous studies, we observed a reduction in the area of

mbl loss-of-function (LOF)

A

	Genotype		L1	L2	L3	L4	L5	Total	no. of OLs
27G05-FLP(X), UAS>stop>epitope	*Dscam2*^{10B}*-Gal4*	+/+	359	0	0	118	0	477	11
	Dscam2^{10A}*-Gal4*	+/+	0	94	105	58	146	403	10
		mbl^{e127}/+	1	96	99	117	147	460	10
		mbl^{MI00976}/+	1	102	114	111	155	483	11
		mbl^{e127}/*mbl*^{MI00976}	45 #	82	105	120	141	493	10

B

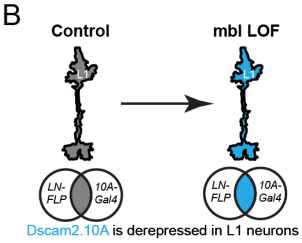

mbl overexpression (OE)

C

	Genotype		L1	L2	L3	L4	L5	Total	no. of OLs
27G05-FLP(X), LexAop>stop>epitope	*Dscam2*^{10A}*-LexA*	*elav-Gal4*	0	57	63	12	89	221	18
	Dscam2^{10B}*-LexA*	*elav-Gal4*	117	0	0	70	0	187	20
		elav-Gal4+UAS-mblB	77	65 #	31 #	29	28 #	230	22

D

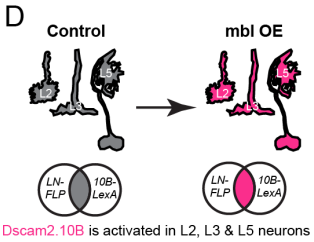

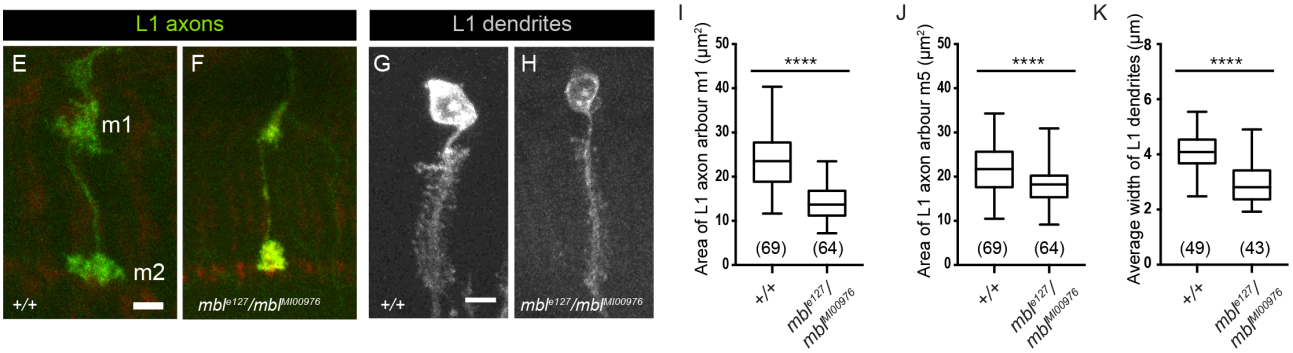

Fig. 5. Mbl regulates *Dscam2* cell-type-specific alternative splicing in lamina neurons. (A) Quantification of lamina neurons L1-L5 observed using the *Dscam2.10B-Gal4* (magenta) or *Dscam2.10A-Gal4* (blue) reporters with the intersectional strategy in *mbl* LOF animals. Green boxes represent high number of labeled neurons. *Dscam2.10A* is de-repressed in L1 neurons in a *mbl* LOF background (*mbl*^{MI00976}/*mbl*^{e27}, hash tag). (B) Schematic of *Dscam2.10A* de-repression in *mbl* LOF L1 neurons. (C) Quantification of lamina neurons L1-L5 observed using the *Dscam2.10A-LexA* (blue) or *Dscam2.10B-LexA* (magenta) reporters with the intersectional strategy in animals with pan-neuronal (elav-Gal4) expression of mbl. Green boxes represent high numbers of labeled neurons. *Dscam2.10B-LexA* was aberrantly detected in L2, L3 and L5 neurons overexpressing *mblB* (hash tag). (D) Schematic of aberrant *Dscam2.10B* selection in L2, L3 and L5 neurons overexpressing *mbl*. (E-K) L1 neurons in *mbl* LOF animals have reduced axon arbor area and dendritic array width when compared to controls. (E) A representative confocal image of a control L1 axon (green) with arbors at m1 and m5 layers. (F) A representative confocal image of an L1 axon from *mbl* LOF animals (*mbl*^{MI00976}/*mbl*^{e27}). (G) A representative confocal image of a control L1 dendritic array (grey). (H) A representative confocal image of a L1 dendritic array from mbl LOF animals (*mbl*^{MI00976}/*mbl*^{e27}). (I) Quantification of L1 axon m1 arbor area (m2). (J) Quantification of L1 axon m5 arbor area (m2). (K) Quantification of L1 dendritic width (m). Tukey boxplot format: middle line = median, range bars = min and max, box = 25–75% quartiles, and each data point = single cartridge. Numbers in parentheses represent total number of L1 neurons quantified. Parametric t-test was used to compare *mbl* LOF L1 axon arbour area with controls. Non-parametric t-test was used to compare *mbl* LOF L1 dendritic width with controls. **** $P < 0.0001$. Bars, 5 microns (E-H).

L1 axon arbors (more prominent in m1 than in m5, Fig 5E-5F and 5I-5J) and the width of dendritic arrays (Fig 5G-5H and 5G) in *mbl* transheterozygous animals (*mbl*^{e127}/*mbl*^{MI00976}) when compared to controls. Finally, we observed a phenotype in MB neurons overexpressing *mbl* where the β lobe neurons inappropriately crossed the midline (Fig S5A-S5C). Interestingly, a similar phenotype was observed in *Dscam2* single isoform mutants. We quantified this phenotype and found that the *Dscam2A*, but not the *Dscam2B*, single isoform line generated a MB fusion phenotype that was significantly different from controls. All of the *UAS-mbl* constructs, except human MBNL1, generated this phenotype at a penetrance that was equal to or greater than *Dscam2A* single isoform lines (Fig S5C). The lack of a phenotype with the human transgene is consistent with this modified isoform having a reduced CUG-binding capacity due to its missing linker domain (Kino et al., 2004; Li et al., 2008). These data demonstrate that MB phenotypes generated in animals overexpressing *mbl*, phenocopy *Dscam2* single isoform mutants. While the origin of this non-autonomous phenotype is not known, it correlates with the misregulation of *Dscam2* alternative isoform expression.

Discussion

In this study, we identify Mbl as a regulator of *Dscam2* alternative splicing. We demonstrate that removing *mbl* in a *mbl*-positive cell-type results in a switch from *Dscam2.10B* to *Dscam2.10A* selection. Ectopic expression of a variety of Mbl protein isoforms in a normally *mbl*-negative neuronal cell-type is sufficient to trigger the selection of *Dscam2.10B*. Consistent with this, transcriptional reporters demonstrate that *mbl* is expressed in a cell-type-specific manner in mul-

tiple cell-types, which tightly correlates with *Dscam2.10B*. Lastly, both the *mbl* LOF and misexpression of *mbl* leads to phenotypes that are observed in flies that express a single *Dscam2* isoform.

Consistent with what has been reported in nematodes (Norris et al., 2017), zebrafish (Machuca-Tzili et al., 2011) and chickens (Huang et al., 2008), we demonstrated cell-type-specific expression of *mbl*. *Mbl* was present in all cells tested that express *Dscam2.10B* and absent from *Dscam2.10A* cells. *Mbl* appears to be regulated at the transcriptional level since the enhancer-trap as well as splicing-trap reporters lack the components crucial for post-transcriptional regulation yet still exhibit cell-type-specific expression (Fig 3). This was unexpected as a recent study showed that *mbl* encodes numerous alternative isoforms that could be individually post-transcriptionally repressed by different microRNAs, thus bypassing the need for transcriptional control of the gene. It will be interesting to explore the in vivo expression patterns of other splicing factors in Drosophila to determine whether cell-specific expression of a subset of splicing factors is a common mechanism for regulating alternative splicing in the brain.

Given that Mbl can repress exon 10A and select exon 10B, it is possible that this single splicing factor and its associated co-factors are sufficient to regulate *Dscam2* cell-specific isoform expression. It could be that *Dscam2.10A* is the default exon selected when the Mbl complex is not present. In this way, cells that express *Dscam2* would be '10A' positive if they did not express *mbl* and '10B' positive if they did. Our RT-PCR data, however, argue that Dscam2 mutually exclusive alternative splicing may be more complicated than this model. In MB α'β' neurons, which select exon 10A, ectopic expression of mbl using *Act5C-Gal4* can switch on a *Dscam2.10B>tdTom* reporter, but the change in isoform expression in the whole brain as measured by RT-PCR is only 8-24% (see Fig 4F). One might expect a more pronounced shift to isoform B if Mbl were the only regulator/mechanism involved. Further studies, including screens for repressors or activators of exon 10B, will be required to resolve this issue.

The L1 axon/dendrite and MB midline crossing defects generated through the LOF and ectopic expression of *mbl*, respectively, support the idea that these phenotypes arise from a disruption in *Dscam2* cell-specific isoform expression. In the lamina, these inappropriate interactions are predicted to occur between L1 and L2 cells, which normally express distinct isoforms. In MBs, however, since both single isoform lines have identical expression patterns (expressed in all *Dscam2*-positive cells), one would expect both lines to exhibit the midline crossing phenotype. Although there is a trend towards increased fusion in animals expressing only *Dscam2.10B* (Fig 4I), it did not reach statistical significance. This issue may have to do with innate differences between isoform A and isoform B that are not completely understood. It is possible that isoform A and B are not identical in terms of signalling due to either differences in homophilic binding or differences in co-factors associated with specific isoforms. Consistent with this notion, we previously reported that *Dscam2.10A* single isoform lines produce stronger phenotypes at photoreceptor synapses compared to *Dscam2.10B* (Kerwin et al., 2018). Another perplexing aspect about the MB phenotype is that it occurs in neurons that either do not express *Dscam2* (β lobe neurons) or express it at such low levels that it is not detectable with our reporters. Thus, the phenotype must arise indirectly. This could occur through inappropriate interactions between α'β' neurons and another non-MB cell type within this brain region that expresses *Dscam2*. Alternatively, this phenotype could be independent of Dscam2 homophilic binding and instead reflect differences in isoform complexes that form in different neurons.

How does Mbl repress *Dscam2.10A* and select *Dscam2.10B* at the level of pre-mRNA? The vertebrate orthologue of Mbl, MBNL1 binds to YCGY (where Y is a pyrimidine) in pre-mRNAs and untranslated regions using its tandem zinc-finger domains, but it is quite promiscuous (Wang et al., 2012). The best-characterized alternative splicing events regulated by MBNL1 are exon skipping or inclusion events. In general, an exon that contains MBNL1 binding sites upstream or within the coding sequence is subject to skipping, whereas downstream binding sites more often promote inclusion (reviewed in Konieczny et al 2014). The mechanisms used by fly Mbl to regulate splicing have not been characterised in detail but given that human MBNL1 can rescue fly *mbl* lethality and promote the endogenous expression of *Dscam2* exon 10B in MBs, presumably the mechanisms are conserved. A simple explanation for how Mbl regulates *Dscam2* mutually exclusive splicing would be that it binds upstream of exon 10A to repress exon inclusion and downstream of exon 10B to promote inclusion. Although there are many potential binding sites for Mbl upstream, downstream and within the alternative exons, an obvious correlation between location and repression vs inclusion is not observed. There is also a large (3kb) intron downstream of exon 10B that could contain cis regulatory elements. In total, there are 63 potential Mbl binding sites (YCGY) within the 5kb variable region of *Dscam2*. Identification of the sequences required for regulation by Mbl will therefore require extensive mapping and ultimately validation using a technique like cross-linking followed by immunoprecipitation (CLIP) (Ule et al., 2003) or TRIBE (McMahon et al., 2016; Xu et al., 2018).

Together, our results demonstrate that selective expression of a splicing factor can drive neuronal cell-type specific alternative splicing. Although mbl is specifically expressed in neurons that express isoform B, it is unlikely that this alternative splicing event is its only purpose in these cells. Rather, it likely regulates the alternative splicing of many other genes crucial for neurodevelopment. Developmental analysis of *mbl* expression in the cells studied here suggests that it turns on after neurons have been specified (similar to Dscam2) and is therefore well suited for regulating processes such as axon guidance and synapse specification. Understanding these splicing events may provide clues into how the brain can diversify its repertoire of proteins that promote neural connectivity.

Experimental Procedures

Fly strains. *Dscam2.10A-LexA* and *Dscam2.10B-LexA* (Tadros et al., 2016), *UAS-Dcr2* and *UAS-mbl-RNAiVDRC28732* (Dietzl et al., 2007), *LexAop-myr-tdTomato* (attP2, (Chen et al., 2014), *UAS-Srp54-RNAiTRiP.HMS03941*, *CadN-RNAiTRiP.HMS02380* and *UAS-mbl-RNAiTRiP.JF03264* (Ni et al., 2008), *UAS-mCD8-GFP* (Lee and Luo, 1999), *FRT42D* (Xu and Rubin, 1993), mbl^{e127} and mbl^{e27}(Begemann et al., 1997), $mbl^{MI00976}$ and $mbl^{MI04093}$ (Venken et al., 2011), *Df(2R)BSC154* (Cook et al., 2012), *Df(2R)Exel6066* (Parks et al., 2004), *ey-FLP* (Chr.1, (Newsome et al., 2000), *GMR-myr-GFP*, mbl^{NP0420}*-Gal4* and mbl^{NP1161}*-Gal4* (Hayashi et al., 2002), mbl^{k01212}*-LacZ* (Spradling et al., 1999), $mbl^{Mi00139}$*-Gal4* (H. Bellen Lab), *Dac-FLP* (Chr.3, (Millard et al., 2007), *UAS>stop>myr::smGdP-V5-THS-UAS>stop>myr::smGdP-cMyc* (attP5, (Nern et al., 2015), *Dscam2.10A-Gal4* and *Dscam2.10B-Gal4* (Lah et al., 2014) *Act5C-Gal4* (Chr.3, from Yash Hiromi), *OK107-Gal4* (Connolly et al., 1996), *UAS-mblA*, *UAS-mblB* and *UAS-mblC* (D. Yamamoto Lab), $PEPmbl^{B2-E1}$, *UAS-mblA-FLAG* and *UAS-MBNL135* (Li et al., 2008).

RNAi screening. The RNAi screen line was generated as follows: *GMR-Gal4* was recombined with *GMR-GFP* on the second chromosome. *Dscam2.10A-LexA* (Tadros et al. 2016) was recombined with *LexAop-myr-tdTomato* on the third chromosome. These flies were crossed together with *UAS-Dcr-2* (X) to make a stable RNAi screen stock. *UAS-RNAi* lines were obtained from Bloomington and VDRC. Lethal *UAS-RNAi* stocks were placed over balancers with developmentally selectable markers. Virgin females were collected from the RNAi screen stock, crossed to UAS-RNAi males and reared at 25°C. Wandering third instar larvae were dissected and fixed. We tested between one to three independent RNAi lines per gene. In total, we imaged ~2300 third instar optic lobes without antibodies using confocal microscopy at 63X. RNAi lines tested are listed in Table S1.

Semiquantitative and quantitative RT-PCR. Total RNA was isolated using TRIzol (Ambion) following the manufacturer's protocol. Reverse transcription was performed on each RNA sample with random primer mix (semiquantitative, NEB) or Oligo-dT (qRT-PCR, NEB) using 200 units of M-MULV (NEB) and 1 µg of RNA in a 20 µL reaction, at 42°C for 1 hr. PCR reactions were set up with specific primers to analyse alternative splicing of various regions of Dscam2. Where possible, semi-quantitative PCR was performed to generate multiple isoforms in a single reaction and relative levels were compared by electrophoresis followed by densitometry. For qRT-PCR, 1µL of CDNA were added to a Luna Universal SYBR-Green qPCR Master Mix kit (NEB). Samples were added into a 200µL 96-well plate and read on the QuantStudio TM 6 Flex Real-Time PCR machine. Rq values were calculated in Excel (Microsoft).

Immunohistochemistry. Immunostaining were conducted as previously described (Lah et al. 2014). Antibody dilutions used were as follows: mouse mAb24B10 (1:20; DSHB), mouse anti-Repo (1:20; DSHB), mouse anti-DAC (1:20; DSHB), mouse anti-Fas2 (1:20; DSHB) rat anti-ELAV (1:200), V5-tag:DyLight anti-mouse 550 (1:500; AbD Serotec), V5-tag:DyLight anti-mouse 405 (1:200; AbD Serotec), myc-tag;DyLight anti-mouse 549 (1:200; AbD Serotec), Phalloidin:Alexa Fluor 568 (1:200; Molecular Probes), DyLight anti-mouse 647 (1:2000; Jackson Laboratory), DyLight Cy3 anti-rat (1:2000; Jackson Laboratory).

Image acquisition. Imaging was performed at the School of Biomedical Sciences Imaging Facility. Images were taken on a Leica SP8 laser scanning confocal system with a 63X Glycerol NA 1.3.

Fly genotypes. Specific genotypes can be found in the supplemental text.

Author contributions

J.S.S.L designed and performed all experiments. S.S.M supervised the project. J.S.S.L and S.S.M wrote the manuscript.

Acknowledgements

We thank Wael Tadros, Yi Chen, Larry Zipursky, Greg Neely, Louis O'Keefe, Nancy Bonini, Aljoscha Nern and Bloomington Stock Center for sharing fly stocks. We thank the Daisuke Yamamoto Lab for constructing the *UAS-mbl* lines deposited and maintained at the Kyoto Stock Center. We thank Shaun Walters for technical assistance on the Leica confocal microscopy. We note that Grace Shin initially observed *Dscam2* isoform expression in the adult mushroom bodies. We thank Kevin Mutemi for his thorough characterization of *Dscam2* isoform expression in mushroom bodies during development and all midline crossing defects in *Dscam2* single isoform mutant animals. We thank Wei Jun Tan for the heroic feat of triple balancing *OK107-Gal4*. We also thank members of the Millard, Pecot, Hilliard and van Swinderen lab for their feedback. The RNAi screen was inspired by the works of Hidehito Kuroyanagi. We thank the Henriques Lab for their LateX template from which this document is constructed upon. This work was supported by the National Health and Medical Research Council of Australia (NHMRC grant APP1021006). J.S.S.L was supported by the Australia Postgraduate Award (Research Training Scheme) from the Australian Federal Government and the Lavidis grant in aid from the School of Biomedical Sciences at the University of Queensland.

References

Artero, R., Prokop, A., Paricio, N., Begemann, G., Pueyo, I., Mlodzik, M., Perez-Alonso, M., and Baylies, M.K. (1998). The muscleblind gene participates in the organization of Z-bands and epidermal attachments of Drosophila muscles and is regulated by Dmef2. Developmental biology 195, 131-143.

Ashwal-Fluss, R., Meyer, M., Pamudurti, N.R., Ivanov, A., Bartok, O., Hanan, M., Evantal, N., Memczak, S., Rajewsky, N., and Kadener, S. (2014). circRNA biogenesis competes with pre-mRNA splicing. Molecular cell 56, 55-66.

Bargiela, A., Llamusi, B., Cerro-Herreros, E., and Artero, R. (2014). Two enhancers control transcription of Drosophila muscleblind in the embryonic somatic musculature and in the central nervous system. PloS one 9, e93125.

Begemann, G., Paricio, N., Artero, R., Kiss, I., Perez-Alonso, M., and Mlodzik, M. (1997). muscleblind, a gene required for photoreceptor differentiation in Drosophila, encodes novel nuclear Cys3His-type zinc-finger-containing proteins. Development 124, 4321-4331.
Bell, T.J., Thaler, C., Castiglioni, A.J., Helton, T.D., and Lipscombe, D. (2004). Cell-specific alternative splicing increases calcium channel current density in the pain pathway. Neuron 41, 127-138.
Blanchette, M., Green, R.E., MacArthur, S., Brooks, A.N., Brenner, S.E., Eisen, M.B., and Rio, D.C. (2009). Genome-wide analysis of alternative pre-mRNA splicing and RNA-binding specificities of the Drosophila hnRNP A/B family members. Molecular cell 33, 438-449.
Brand, A.H., and Perrimon, N. (1993). Targeted gene expression as a means of altering cell fates and generating dominant phenotypes. Development 118, 401-415.
Brouwer, J., Nagelkerke, D., den Heijer, P., Ruiter, J.H., Mulder, H., Begemann, M.J., and Lie, K.I. (1997). Analysis of atrial sensed far-field ventricular signals: a reassessment. Pacing and clinical electrophysiology : PACE 20, 916-922.
Calarco, J.A., Superina, S., O'Hanlon, D., Gabut, M., Raj, B., Pan, Q., Skalska, U., Clarke, L., Gelinas, D., van der Kooy, D., et al. (2009). Regulation of vertebrate nervous system alternative splicing and development by an SR-related protein. Cell 138, 898-910.
Chen, Y., Akin, O., Nern, A., Tsui, C.Y., Pecot, M.Y., and Zipursky, S.L. (2014). Cell-type-specific labeling of synapses in vivo through synaptic tagging with recombination. Neuron 81, 280-293.
Connolly, J.B., Roberts, I.J., Armstrong, J.D., Kaiser, K., Forte, M., Tully, T., and O'Kane, C.J. (1996). Associative learning disrupted by impaired Gs signaling in Drosophila mushroom bodies. Science 274, 2104-2107.
Cook, R.K., Christensen, S.J., Deal, J.A., Coburn, R.A., Deal, M.E., Gresens, J.M., Kaufman, T.C., and Cook, K.R. (2012). The generation of chromosomal deletions to provide extensive coverage and subdivision of the Drosophila melanogaster genome. Genome biology 13, R21.
Diao, F., Ironfield, H., Luan, H., Diao, F., Shropshire, W.C., Ewer, J., Marr, E., Potter, C.J., Landgraf, M., and White, B.H. (2015). Plug-and-play genetic access to drosophila cell types using exchangeable exon cassettes. Cell reports 10, 1410-1421.
Dietzl, G., Chen, D., Schnorrer, F., Su, K.C., Barinova, Y., Fellner, M., Gasser, B., Kinsey, K., Oppel, S., Scheiblauer, S., et al. (2007). A genome-wide transgenic RNAi library for conditional gene inactivation in Drosophila. Nature 448, 151-U151.
Funada, M., Hara, H., Sasagawa, H., Kitagawa, Y., and Kadowaki, T. (2007). A honey bee Dscam family member, AbsCAM, is a brain-specific cell adhesion molecule with the neurite outgrowth activity which influences neuronal wiring during development. The European journal of neuroscience 25, 168-180.
Hayashi, S., Ito, K., Sado, Y., Taniguchi, M., Akimoto, A., Takeuchi, H., Aigaki, T., Matsuzaki, F., Nakagoshi, H., Tanimura, T., et al. (2002). GETDB, a database compiling expression patterns and molecular locations of a collection of Gal4 enhancer traps. Genesis 34, 58-61. Houseley, J.M., Garcia-Casado, Z., Pascual, M., Paricio, N.,
O'Dell, K.M., Monckton, D.G., and Artero, R.D. (2006). Noncanonical RNAs from transcripts of the Drosophila muscleblind gene. The Journal of heredity 97, 253-260.
Huang, H., Wahlin, K.J., McNally, M., Irving, N.D., and Adler, R. (2008). Developmental regulation of muscleblind-like (MBNL) gene expression in the chicken embryo retina. Developmental dynamics : an official publication of the American Association of Anatomists 237, 286-296.
Iijima, T., Iijima, Y., Witte, H., and Scheiffele, P. (2014). Neuronal cell type-specific alternative splicing is regulated by the KH domain protein SLM1. The Journal of cell biology 204, 331-342.
Irion, U. (2012). Drosophila muscleblind codes for proteins with one and two tandem zinc finger motifs. PloS one 7, e34248.
Juni, N., and Yamamoto, D. (2009). Genetic analysis of chaste, a new mutation of Drosophila melanogaster characterized by extremely low female sexual receptivity. Journal of neurogenetics 23, 329-340.
Kania, A., Salzberg, A., Bhat, M., D'Evelyn, D., He, Y., Kiss, I., and Bellen, H.J. (1995). P-element mutations affecting embryonic peripheral nervous system development in Drosophila melanogaster. Genetics 139, 1663-1678.
Kerwin, S.K., Li, J.S.S., Noakes, P.G., Shin, G.J., and Millard, S.S. (2018). Regulated Alternative Splicing of Drosophila Dscam2 Is Necessary for Attaining the Appropriate Number of Photoreceptor Synapses. Genetics 208, 717-728.
Kino, Y., Mori, D., Oma, Y., Takeshita, Y., Sasagawa, N., and Ishiura, S. (2004). Muscleblind protein, MBNL1/EXP, binds specifically to CHHG repeats. Human molecular genetics 13, 495-507.
Kuroyanagi, H., Kobayashi, T., Mitani, S., and Hagiwara, M. (2006). Transgenic alternative-splicing reporters reveal tissue-specific expression profiles and regulation mechanisms in vivo. Nature methods 3, 909-915.
Lah, G.J., Li, J.S., and Millard, S.S. (2014). Cell-specific alternative splicing of Drosophila Dscam2 is crucial for proper neuronal wiring. Neuron 83, 1376-1388.
Lai, S.L., and Lee, T. (2006). Genetic mosaic with dual binary transcriptional systems in Drosophila. Nature neuroscience 9, 703-709.
Lee, T., and Luo, L. (1999). Mosaic analysis with a repressible cell marker for studies of gene function in neuronal morphogenesis. Neuron 22, 451-461.
Li, J.S., Shin, G.J., and Millard, S.S. (2015). Neuronal cell-type-specific alternative splicing: A mechanism for specifying connections in the brain? Neurogenesis 2, e1122699.
Li, L.B., Yu, Z., Teng, X., and Bonini, N.M. (2008). RNA toxicity is a component of ataxin-3 degeneration in Drosophila. Nature 453, 1107-1111.
Llamusi, B., Bargiela, A., Fernandez-Costa, J.M., Garcia-Lopez, A., Klima, R., Feiguin, F., and Artero, R. (2013). Muscleblind, BSF and TBPH are mislocalized in the muscle sarcomere of a Drosophila myotonic dystrophy model. Disease models & mechanisms 6, 184-196.
Machuca-Tzili, L.E., Buxton, S., Thorpe, A., Timson, C.M., Wigmore, P., Luther, P.K., and Brook, J.D. (2011). Zebrafish deficient for Muscleblind-like 2 exhibit features of myotonic dystrophy. Disease models & mechanisms 4, 381-392.
Markovtsov, V., Nikolic, J.M., Goldman, J.A., Turck, C.W., Chou, M.Y., and Black, D.L. (2000). Cooperative assembly of an hnRNP complex induced by a tissue-specific homolog of polypyrimidine tract binding protein. Molecular and cellular biology 20, 7463-7479.
McKee, A.E., Minet, E., Stern, C., Riahi, S., Stiles, C.D., and Silver, P.A. (2005). A genome-wide in situ hybridization map of RNA-binding proteins reveals anatomically restricted expression in the developing mouse brain. BMC developmental biology 5, 14.
McMahon, A.C., Rahman, R., Jin, H., Shen, J.L., Fieldsend, A., Luo, W., and Rosbash, M. (2016). TRIBE: Hijacking an RNA-Editing Enzyme to Identify Cell-Specific Targets of RNA-Binding Proteins. Cell 165, 742-753.
Millard, S.S., Flanagan, J.J., Pappu, K.S., Wu, W., and Zipursky, S.L. (2007). Dscam2 mediates axonal tiling in the Drosophila visual system. Nature 447, 720-724.
Millard, S.S., Lu, Z., Zipursky, S.L., and Meinertzhagen, I.A. (2010). Drosophila dscam proteins regulate postsynaptic specificity at multiple-contact synapses. Neuron 67, 761-768.
Mondal, K., VijayRaghavan, K., and Varadarajan, R. (2007). Design and utility of temperature-sensitive Gal4 mutants for conditional gene expression in Drosophila. Fly 1, 282-286.
Nern, A., Pfeiffer, B.D., and Rubin, G.M. (2015). Optimized tools for multicolor stochastic labeling reveal diverse stereotyped cell arrangements in the fly visual system. Proceedings of the National Academy of Sciences of the United States of America 112, E2967-E2976.
Newsome, T.P., Schmidt, S., Dietzl, G., Keleman, K., Asling, B., Debant, A., and Dickson, B.J. (2000). Trio combines with dock to regulate Pak activity during photoreceptor axon pathfinding in Drosophila. Cell 101, 283-294.
Ni, J.Q., Markstein, M., Binari, R., Pfeiffer, B., Liu, L.P., Villalta, C., Booker, M., Perkins, L., and Perrimon, N. (2008). Vector and parameters for targeted transgenic RNA interference in Drosophila melanogaster. Nature methods 5, 49-51.
Nilsen, T.W., and Graveley, B.R. (2010). Expansion of the eukaryotic proteome by alternative splicing. Nature 463, 457-463.
Norris, A.D., Gao, S., Norris, M.L., Ray, D., Ramani, A.K., Fraser, A.G., Morris, Q., Hughes, T.R., Zhen, M., and Calarco, J.A. (2014). A pair of RNA-binding proteins controls networks of splicing events contributing to specialization of neural cell types. Molecular cell 54, 946-959. Norris, A.D., Gracida, X., and Calarco, J.A. (2017). CRISPR-mediated genetic interaction profiling identifies RNA binding proteins controlling metazoan fitness. eLife 6.
Ohno, G., Hagiwara, M., and Kuroyanagi, H. (2008). STAR family RNA-binding protein ASD-2 regulates developmental switching of mutually exclusive alternative splicing in vivo. Genes & development 22, 360-374.
Pan, Q., Shai, O., Lee, L.J., Frey, B.J., and Blencowe, B.J. (2008). Deep surveying of alternative splicing complexity in the human transcriptome by high-throughput sequencing. Nature genetics 40, 1413-1415.
Parks, A.L., Cook, K.R., Belvin, M., Dompe, N.A., Fawcett, R., Huppert, K., Tan, L.R., Winter, C.G., Bogart, K.P., Deal, J.E., et al. (2004). Systematic generation of high-resolution deletion coverage of the Drosophila melanogaster genome. Nature genetics 36, 288-292.
Pascual, M., Vicente, M., Monferrer, L., and Artero, R. (2006). The Muscleblind family of proteins: an emerging class of regulators of developmentally programmed alternative splicing. Differentiation; research in biological diversity 74, 65-80.
Schreiner, D., Nguyen, T.M., Russo, G., Heber, S., Patrignani, A., Ahrne, E., and Scheiffele, P. (2014). Targeted combinatorial alternative splicing generates brain region-specific repertoires of neurexins. Neuron 84, 386-398.
Spradling, A.C., Stern, D., Beaton, A., Rhem, E.J., Laverty, T., Mozden, N., Misra, S., and Rubin, G.M. (1999). The Berkeley Drosophila Genome Project gene disruption project: Single P-element insertions mutating 25% of vital Drosophila genes. Genetics 153, 135-177.
Tadros, W., Xu, S.W., Akin, O., Yi, C.H., Shin, G.J.E., Millard, S.S., and Zipursky, S.L. (2016). Dscam Proteins Direct Dendritic Targeting through Adhesion. Neuron 89, 480-493.
Tan, L., Zhang, K.X., Pecot, M.Y., Nagarkar-Jaiswal, S., Lee, P.T., Takemura, S.Y., McEwen, J.M., Nern, A., Xu, S., Tadros, W., et al. (2015). Ig Superfamily Ligand and Receptor Pairs Expressed in Synaptic Partners in Drosophila. Cell 163, 1756-1769.
Tomioka, M., Naito, Y., Kuroyanagi, H., and Iino, Y. (2016). Splicing factors control C. elegans behavioural learning in a single neuron by producing DAF-2c receptor. Nature communications 7, 11645. Ule, J., Jensen, K.B., Ruggiu, M., Mele, A., Ule, A., and Darnell, R.B. (2003). CLIP identifies Nova-regulated RNA networks in the brain. Science 302, 1212-1215.
Underwood, J.G., Boutz, P.L., Dougherty, J.D., Stoilov, P., and Black, D.L. (2005). Homologues of the Caenorhabditis elegans Fox-1 protein are neuronal splicing regulators in mammals. Molecular and cellular biology 25, 10005-10016. Venken, K.J., Schulze, K.L., Haelterman, N.A., Pan, H., He, Y., Evans-Holm, M.,
Carlson, J.W., Levis, R.W., Spradling, A.C., Hoskins, R.A., and Bellen, H.J. (2011). MiMIC: a highly versatile transposon insertion resource for engineering Drosophila melanogaster genes. Nature methods 8, 737-743.
Vicente, M., Monferrer, L., Poulos, M.G., Houseley, J., Monckton, D.G., O'Dell K, M., Swanson, M.S., and Artero, R.D. (2007). Muscleblind isoforms are functionally distinct and regulate alpha-actinin splicing. Differentiation; research in biological diversity 75, 427-440.
Wang, E.T., Cody, N.A., Jog, S., Biancolella, M., Wang, T.T., Treacy, D.J., Luo, S., Schroth, G.P., Housman, D.E., Reddy, S., et al. (2012). Transcriptome-wide regulation of pre-mRNA splicing and mRNA localization by muscleblind proteins. Cell 150, 710-724.

Wang, E.T., Sandberg, R., Luo, S., Khrebtukova, I., Zhang, L., Mayr, C., Kingsmore, S.F., Schroth, G.P., and Burge, C.B. (2008). Alternative isoform regulation in human tissue transcriptomes. Nature 456, 470-476.
Wang, Q., Abruzzi, K.C., Rosbash, M., and Rio, D.C. (2018). Striking circadian neuron diversity and cycling of Drosophila alternative splicing. eLife 7.
Warzecha, C.C., Sato, T.K., Nabet, B., Hogenesch, J.B., and Carstens, R.P. (2009). ESRP1 and ESRP2 are epithelial cell-type-specific regulators of FGFR2 splicing. Molecular cell 33, 591-601.
Xu, T., and Rubin, G.M. (1993). Analysis of genetic mosaics in developing and adult Drosophila tissues. Development 117, 1223-1237.
Xu, W., Rahman, R., and Rosbash, M. (2018). Mechanistic implications of enhanced editing by a HyperTRIBE RNA-binding protein. Rna 24, 173-182.

Supplemental Information

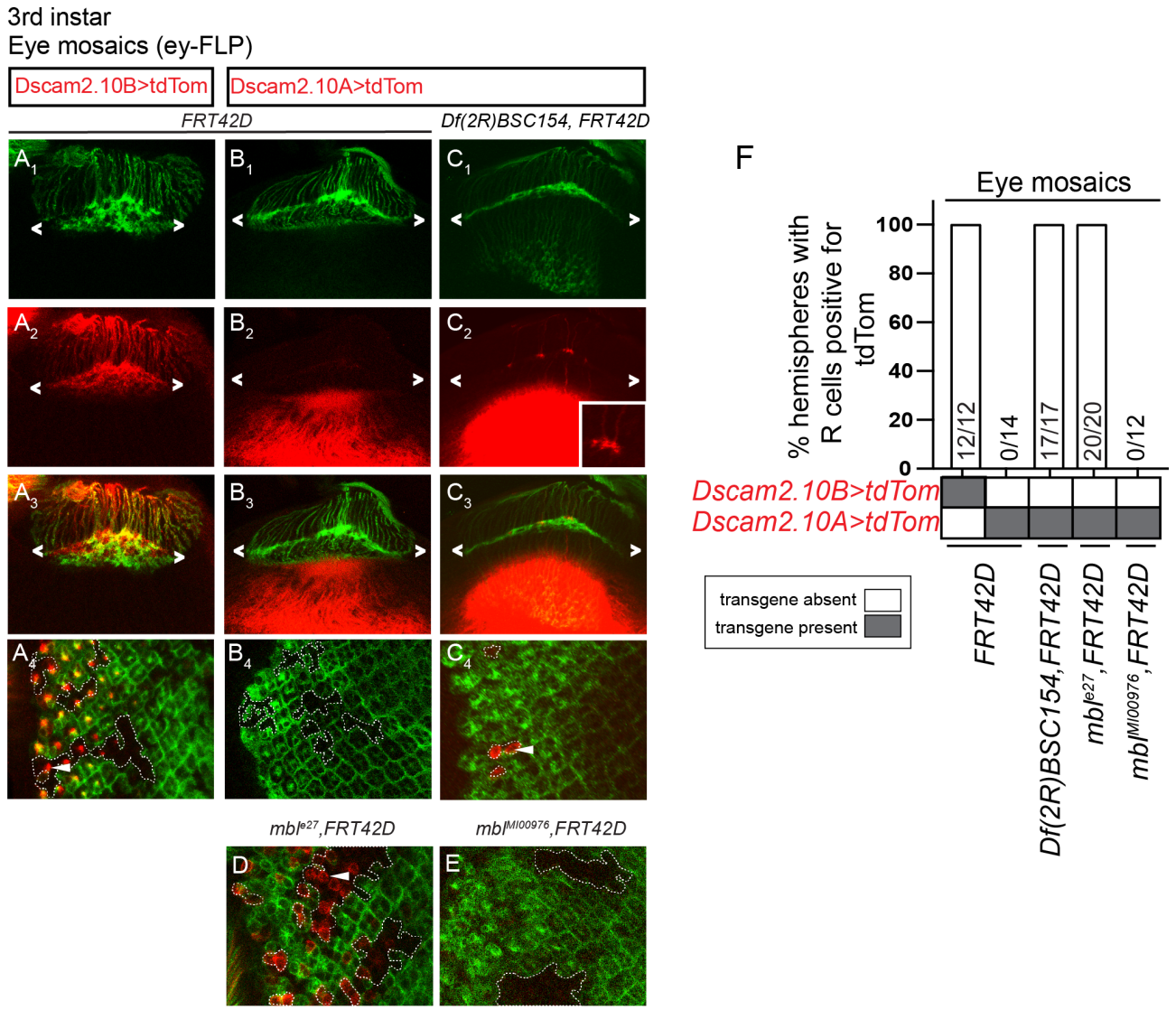

Fig. S1. Related to Figure 1. *Mbl* LOF results in aberrant *Dscam2.10A* reporter expression in eye mosaic clones. (A-F) Eye mosaics of *mbl* LOF alleles cause de-repression of *Dscam2.10A>tdTom* in R cells. WT mosaic clones (GFP-negative) express *Dscam2.10B>tdTom* (A_1-A_4) but not *Dscam2.10A>tdTom* (B_1-B_4). *Mbl* mutant (GFP-negative) clones, *Df(2R)BSC154* show aberrant *Dscam2.10A* expression in R cells (C_1-C_4). (D) mbl^{e27} eye clones exhibit de-repression of Dscam2.10A (red). (E) Clones of a *mbl* allele that deleted only a portion of all *mbl* isoforms ($mbl^{MI00976}$) do not exhibit de-repression of *Dscam2.10A*. (F) Quantification of *Dscam2.10>tdTom* expression in third instar R cells with *mbl* LOF eye mosaic clones. Y-axis represents the number of optic lobes with R cells positive for tdTom over total number of optic lobes quantified as a percentage. On the x-axis, the presence of a transgene is indicated with a grey box.

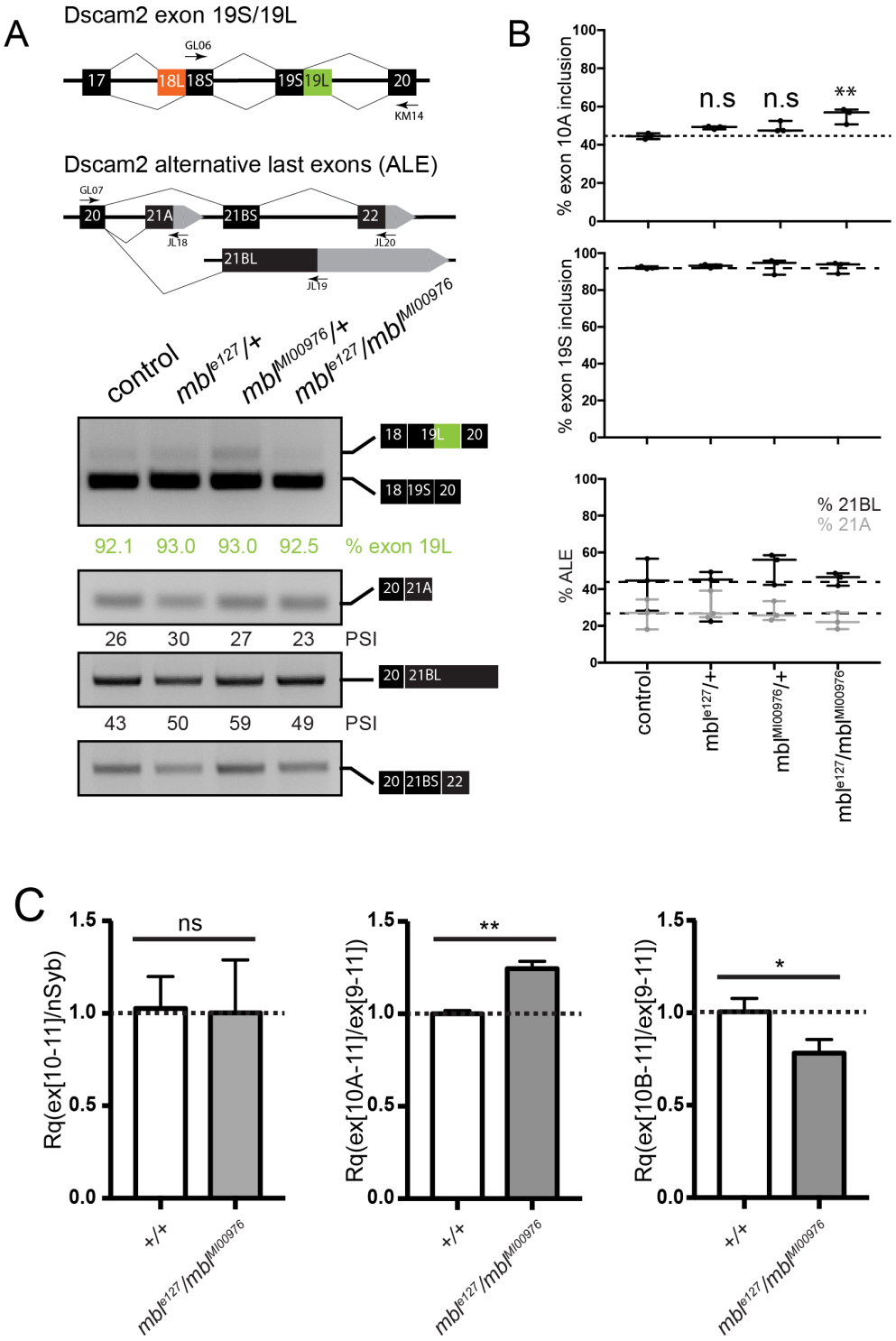

Fig. S2. Related to Figure 1. *Mbl* LOF is associated with increased *Dscam2.10A* inclusion without affecting other *Dscam2* splicing events. (A) *Mbl* LOF ($mbl^{e127}/mbl^{MI00976}$) does not affect other *Dscam2* splicing events. Semiquantitative RT-PCR from different genotypes indicated. Primers amplified the variable region that includes exon 19S/19L or three alternative last exons (ALE). Percentage of 19L inclusion was calculated by dividing the 19L band by 19L+19S. Percentage of ALE 21A and ALE 21BL inclusion was calculated by dividing respectively the 21A and 21BL band by 21A+21BL+21BS (total). (B) Graphs of RT-PCR data from A and Figure 1P. Top graph depicts *Dscam2.10A* inclusion. Middle graph represents exon 19S inclusion. Bottom graph represents percentage inclusion of different ALEs. Plots show minimum (bottom line), mean (middle line) and maximum (top line) points, where individual points depict biological replicates. Dashed line represents mean of control. (C) Quantitative RT-PCR of *mbl* LOF mutant ($mbl^{e127}/mbl^{MI00976}$) show increased exon 10A inclusion and decreased exon 10B inclusion. The left graph shows *Dscam2.10* levels compared to synaptobrevin (nSyb). The middle graph shows *Dscam2.10A* levels compared to *Dscam2.10*. The right graph shows *Dscam2.10B* levels compared to Dscam2. Bar graph format (error bars depict standard error of means). The y-axis is the relative quantity (Rq). Dashed line represents mean of control. Unpaired t-test was conducted to compare Rq levels between control and *mbl* LOF mutants. ns $P > 0.05$, * $P < 0.05$, ** $P < 0.01$.

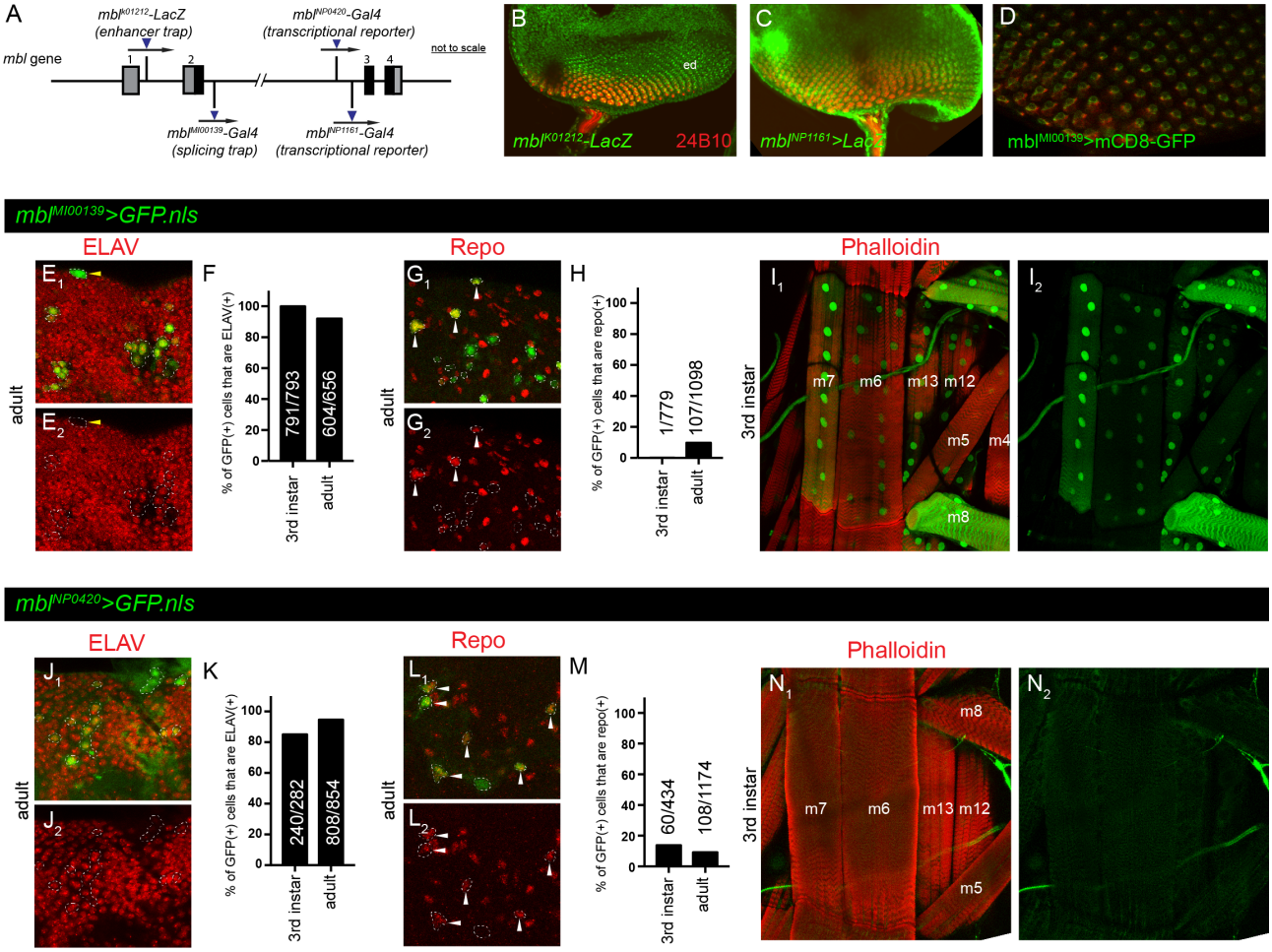

Fig. S3. Related to Figure 3. *Mbl* is expressed in R cells, neurons and glia (A) Schematic showing the insertion locations of different *mbl* reporters. Translated regions (black) and non-translated regions (grey) are shown. (B-D) *Mbl* is expressed in R cells (red) in third instar eye-discs (ed). The *mbl* enhancer traps *mbl*^{K01212}*-LacZ* (B), *mbl*^{NP1161}*-Gal4* (C) and splicing trap reporter *mbl*^{MI00139}*-Gal4* (D, green) overlapped with a marker of R cells (24B10). (E-I) *mbl*^{MI00139}*>GFP.nls* is expressed in neurons and muscles. (E_1-E_2) Representative confocal image of a *mbl*^{MI00139}*>GFP.nls* (green) adult brain co-labeled with an ELAV antibody (red). Dashed lines demarcate GFP(+) cells. Yellow solid arrowheads show GFP(+) cells that are ELAV(-). (F) Quantification of *mbl* in third instar and adult brains where 90-100% of GFP(+) cells are also ELAV(+) (black bars). Y-axis represents the number of GFP(+) cells positive for ELAV quantified as a percentage. (G_1-G_2) Representative confocal image of a *mbl*^{MI00139}*>GFP.nls* adult brain labeled with a Repo antibody (red). Dashed lines demarcate GFP(+) cells. White solid arrowheads show GFP(+) cells that are positive for Repo. (H) Quantification of *mbl*^{MI00139}*>GFP.nls* where 0-10% of *mbl*^{MI00139}*>GFP.nls* (+) cells are also Repo(+).Y-axis represents the number of GFP(+) cells positive for Repo quantified as a percentage. (I_1-I_2) *mbl*^{MI00139}*>GFP.nls* expression is also found in third instar muscles m4-m8, m12 and m13 (Phalloidin, red). (J_1-J_2) Representative confocal image of a *mbl*^{NP0420}*>GFP.nls* (green) adult brain co-labeled with an ELAV antibody (red). Dashed lines demarcate GFP(+) cells. (K) Quantification of *mbl*^{NP0420}*>GFP.nls* in third instar and adult brains where 80-90% of GFP(+) cells are also ELAV(+). (L-M) In third instar and adult brains, *mbl*^{NP0420}*>GFP.nls* overlaps minimally with Repo (red). (L_1-L_2) Representative confocal image of a *mbl*^{NP0420}*>GFP.nls* adult brain labeled with Repo. Dashed lines demarcate GFP(+) cells. White solid arrowheads show GFP(+) cells that are positive for Repo. (M) Quantification of *mbl*^{NP0420}*>GFP.nls* in third instar and adult brains where 10-15% of GFP (+) cells are also Repo(+). (N_1-N_2) *mbl*^{NP0420}*>GFP.nls* expression is not detected in third instar muscles m4-m8, m12 and m13 (Phalloidin, red).

A

Genotype			L1	L2	L3	L4	L5	R7	R8	Total	no. of OLs
Dac-FLP(III), UAS>stop>epitope	mbl^{NP0420}-Gal4	72 apf	75	0	0	10	0	10	38	133	8
		60 apf	22	0	0	8	0	15	29	74	8
		48 apf	7	0	0	3	0	1	9	20	2
	$mbl^{MI00139}$-Gal4	72 apf	15	0	0	0	0	6	15	36	8
		48 apf	12	0	0	0	0	4	24	40	8

Clones detected
No clones detected

B

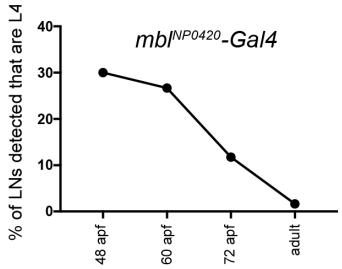

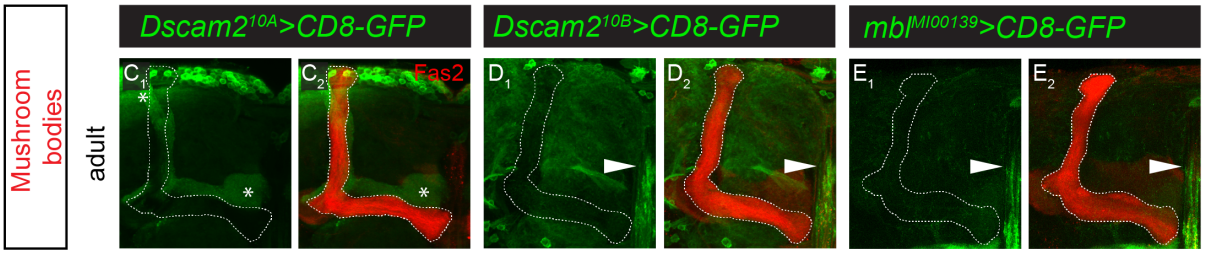

Fig. S4. Related to Figure 3. *Mbl* expression is cell-type-specific and correlates with *Dscam2.10B*. (A) Quantification of lamina neurons and R7-R8 neurons observed using the intersectional strategy during development. Two different *mbl* reporters were used. The transcriptional reporter labeled L4 cells early in development whereas the splicing trap reporter did not. This is most likely due to the lower efficiency of the splicing trap given that it produced 5X fewer L1 clones at 72hr compared to the transcriptional reporter. Green boxes represent detection of reporter expression at different hours after pupal formation (apf). (B) A plot of the percentage of L4 lamina neurons over total lamina neurons during development (data from the *mbl* transcriptional reporter). (C-E) *Mbl* is not detected in MB neurons that express Dscam2.10A in adults. (C_1-C_2) *Dscam2.10A* is expressed in α'β' mushroom body neurons (asterisks) but not the αβ and subsets of MB neurons labeled by Fas2 (red). Neither *Dscam2.10B* (D_1-D_2) nor mbl (E_1-E_2) are expressed in MB neurons. Neurons in the midline express both *Dscam2.10B* and *mbl* (white arrowhead).

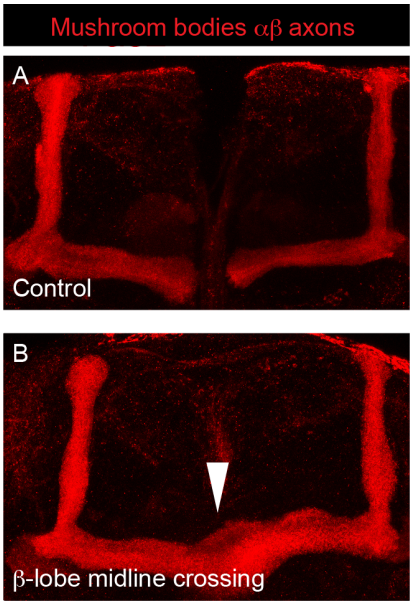

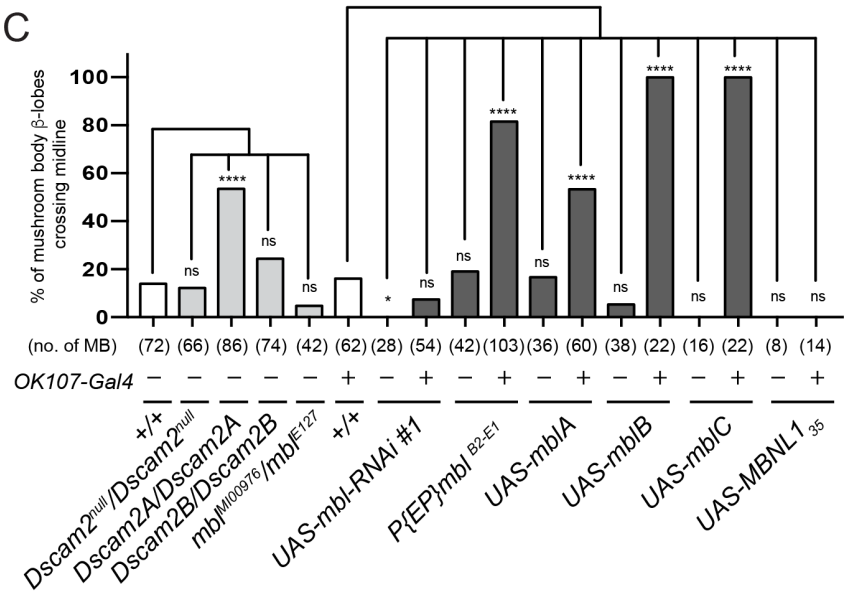

Fig. S4. Related to Figure 4. Neurons overexpressing *mbl* phenocopy *Dscam2* single isoform mutants (A-B) MBs overexpressing *mbl* exhibit defects associated with *Dscam2* single isoform mutants. (A) A representative confocal image of control adult αβ lobes (red) with clear separation between the two β-lobes at the midline. (B) A representative confocal image of adult αβ lobes from an animal overexpressing *mblA*. β-lobe axons inappropriately cross the midline (arrowhead). (C) Quantification of β-lobe axon midline crossing defects. Numbers in parentheses represent total number of MBs quantified. Fishers exact test was used to compare genotypes to their corresponding controls (white bars). ns $P > 0.05$, * $P < 0.05$ and **** $P < 0.0001$.

Table S1. List of tested RNAi that did not de-repress Dscam2 exon 10A in R cells

Flybase Number	CG Number	Gene Name	RNAi ID	no. of ol/ed	no. of animals
FBgn0052062	CG32062	A2bp1	27286	12	6
FBgn026239	CG6671	AGO1	33727	3	2
FBgn0000114	CG31762	aret	44483	18	9
FBgn0004587	CG10851	B52	v38862	16	8
FBgn0004587	CG10851	B52	v38860	4	2
FBgn0037660	CG18005	bcag	v103832	8	4
FBgn0015907	CG13425	bl	v2912	10	6
FBgn0015907	CG13425	bl	v105271	9	5
FBgn0262475	CG6319	bru-2	50631	13	7
FBgn0264001	CG43744	Bru-3	50734	8	4
FBgn0031883	CG11266	Caper	55742	10	6
FBgn0031883	CG11266	Caper	55742	8	4
FBgn0022942	CG7035	Cbp80	v22331	12	8
FBgn0035136	CG6905	Cdc5	v13492	2	1
FBgn0035136	CG6905	Cdc5	v109369	10	5
FBgn0032690	CG10333	CG10333	v18132	12	8
FBgn0032690	CG10333	CG10333	v18133	4	2
FBgn0036277	CG10418	CG10418	v105940	11	6
FBgn0037531	CG10445	CG10445	v104753	14	7
FBgn0036314	CG10754	CG10754	v31346	11	8
FBgn0039920	CG11360	CG11360	v38491	15	8
FBgn0039920	CG11360	CG11360	v38492	11	6
FBgn0035692	CG13298	CG13298	55257	8	4
FBgn0035162	CG13900	CG13900	v18955	9	6
FBgn0035163	CG13900	CG13900	v108248	16	8
FBgn0037220	CG14641	CG14641	v110507/CyOtb	11	6
FBgn0038464	CG16941	CG16941	v20338	1	1
FBgn0033089	CG17266	CG17266	v25243	10	5
FBgn0033089	CG17266	CG17266	v25244	2	1
FBgn0029751	CG17764	CG17764	v20541	12	7
FBgn0029751	CG17764	CG17764	v101894	10	5
FBgn0035271	CG2021	CG2021	28579	8	5
FBgn0031266	CG2807	CG2807	v25162	8	5
FBgn0037344	CG2926	CG2926	v33589	11	5
FBgn050122	CG30122	CG30122	55209	6	3
FBgn0031631	CG3225	CG3225	v24725	9	5
FBgn0052533	CG32533	CG32533	v38634	1	1
FBgn0052533	CG32533	CG32533	v51785	11	6
FBgn0031628	CG3294	CG3294	v26111/TM6B	12	6
FBgn0031628	CG3294	CG3294	v26111/TM6B	12	6
FBgn0053108	CG33108	CG33108	v24996	9	5
FBgn0031229	CG3436	CG3436	55207/CyOtb	4	2
FBgn0031492	CG3542	CG3542	v26227	10	5
FBgn0031492	CG3542	CG3542	v26229	4	2
FBgn0031493	CG3605	CG3605	v26250	12	7
FBgn0031493	CG3605	CG3605	v26252	8	5
FBgn0035987	CG3689	CG3689	v45278	10	5
FBgn0028474	CG4119	CG4119	v26395	9	5
FBgn0028474	CG4119	CG4119	v106696/CyOtb	10	6
FBgn0034598	CG4266	CG4266	v26472	14	7
FBgn0034598	CG4266	CG4266	v26475	4	2
FBgn0031287	CG4291	CG4291	v21819/TM6B	11	6
FBgn0035016	CG4612	CG4612	v52497	9	5
FBgn0039566	CG4849	CG4849	v21962	9	5
FBgn0032194	CG4901	CG4901	v34904	11	6
FBgn0038344	CG5205	CG5205	v107282	9	5
FBgn0039182	CG5728	CG5728	v24697	14	7
FBgn0038927	CG6015	CG6015	34565	lethal	
FBgn0030631	CG6227	CG6227	v40351	11	8
FBgn0030632	CG6227	CG6227	v40352	12	6
FBgn0004903	CG6354	CG6354	31333	12	9
FBgn0004903	CG6354	CG6354	55662	8	4
FBgn0035675	CG6610	CG6610	v106830	10	6
FBgn0035675	CG6610	CG6610	31870	10	6
FBgn0036828	CG6841	CG6841	v34253/CyOtb	10	5
FBgn0030085	CG6999	CG6999	v110143	11	7
FBgn0030085	CG6999	CG6999	55157	12	6
FBgn0035872	CG7185	CG7185	v107147	5	3
FBgn0035872	CG7185	CG7185	34804	14	7
FBgn0036734	CG7564	CG7564	v100562	10	5
FBgn0035235	CG7879	CG7879	56930	10	5
FBgn0038887	CG7907	CG7907	55370	6	3
FBgn0035253	CG7971	CG7971	v101384	10	7
FBgn0027567	CG8108	CG8108	v35344	12	7
FBgn0030697	CG8565	CG8565	v100449	10	7
FBgn0030697	CG8565	CG8565	55368	11	6
FBgn0032883	CG9323	CG9323	v44984	12	8
FBgn0032883	CG9323	CG9323	v110410	8	4
FBgn0015621	CG3642	Clp	v26259	12	7
FBgn0015621	CG3642	Clp	v26261	13	7
FBgn0263995	CG43738	cpo	28360	8	4
FBgn0027873	CG1957	Cpsf100	50893/TM6B	8	5
FBgn0027873	CG1957	Cpsf100	50893/TM6B	8	5
FBgn0024698	CG10110	Cpsf160	v18009	11	6
FBgn0024698	CG10110	Cpsf160	v110571	9	6
FBgn0261065	CG7698	Cpsf73	v39558	9	5
FBgn0000377	CG3193	crn	v25919	lethal	
FBgn0039867	CG2261	CstF-50	v43716	10	5
FBgn0039867	CG2261	CstF-50	v109583	8	4
FBgn0027841	CG7697	CstF-64	v21045/CyOtb	10	6
FBgn0010220	CG12759	Dbp45A	v17306	6	3
FBgn0010221	CG12760	Dbp45A	v104183	13	7
FBgn0033160	CG11107	Dhx15	v44119/CyOtb	10	6
FBgn0031601	CG3058	Dim1	v21258	10	5
FBgn0259220	CG42320	Doa	v19066	9	5
FBgn0020306	CG9696	dom	v7787	2	1
FBgn0000562	CG4051	egl	28969	8	4
FBgn0001942	CG9075	eIF-4a	v42202	lethal	
FBgn0034237	CG4878	eIF3-S9	32880	lethal	
FBgn0260400	CG4262	elav	28371	2	1
FBgn0033859	CG6197	fand	v104186	10	5
FBgn0036850	CG10419	Gem2	v47372	13	8
FBgn0036850	CG10419	Gem2	v47374	10	7
FBgn0259139	CG6946	glo	33668	9	6
FBgn0259139	CG6946	glo	v27752	12	6
FBgn0001179	CG8019	hay	v41023	12	8
FBgn0014189	CG7269	Hel25E	v22557	9	5
FBgn0011224	CG31000	heph	v33735	10	6
FBgn0011224	CG31000	heph	v110749	18	10
FBgn0264491	CG10293	how	v13756	13	7
FBgn0264491	CG10293	how	v100775	10	5
FBgn0004838	CG10377	Hrb27c, Hrp48	v16040	12	7
FBgn0004838	CG10377	Hrb27c, Hrp48	31685	6	3
FBgn0004838	CG10377	Hrb27c, Hrp48	33716	8	4
FBgn0004237	CG12749	Hrb87F, hrp36	v51759	9	6
FBgn0004237	CG12749	Hrb87F, hrp36	52937	11	6
FBgn0004237	CG12749	Hrb87F, hrp36	31244	14	8
FBgn0001215	CG9983	Hrb98DE, hrp38	31303	10	7
FBgn0001215	CG9983	Hrb98DE, hrp38	32351	13	8
FBgn0015949	CG9854	hrg	v42283	12	6
FBgn0002431	CG9484	hyd	v44675	12	6
FBgn0039691	CG1972	IntS11	v33450	7	5
FBgn0039691	CG1972	IntS11	v109408	8	5
FBgn0036570	CG5222	IntS9	v110367	10	5
FBgn0026713	CG32604	l(1)G0007	v31908	15	8
FBgn0026714	CG32605	l(1)G0008	v31909	4	2
FBgn0086444	CG10689	l(2)37Cb	v31324	9	6
FBgn0263599	CG5931	l(3)72Ab	v43962	5	3
FBgn0263600	CG5932	l(3)72Ab	v110666	6	3
FBgn0035838	CG7942	ldbr	v110582	8	5
FBgn0035838	CG7942	ldbr	55661	8	6
FBgn0034834	CG3162	LS2	v21379	11	7
FBgn0034834	CG3162	LS2	v21380	14	7
FBgn0261067	CG4279	LSm1	v28793	11	6
FBgn0261067	CG4279	LSm1	v50653	10	5
FBgn0033450	CG12924	Lsm11	v108336	12	6
FBgn0051184	CG31184	LSm3	56892	4	2
FBgn0261068	CG13277	Lsm7	v23862	10	6
FBgn0011666	CG5099	msi	55152	10	5
FBgn0262737	CG7437	mub	v28024	16	9
FBgn0014366	CG2925	noi	v20943	9	5
FBgn0015520	CG10328	nonA-I	v101567	7	4
FBgn0015520	CG10328	nonA-I	52934	3	2
FBgn0261619	CG5119	pAbp	v22007	9	5
FBgn0005648	CG2163	Pabp2	v106466	10	5
FBgn0086895	CG8241	pea	v47782	9	5
FBgn0027784	CG6011	Prp18	v13760	10	6
FBgn0027784	CG6011	Prp18	v100287	2	1
FBgn0261119	CG5519	Prp19	v108575	11	6
FBgn0261119	CG5519	Prp19	v41438	3	2
FBgn0036915	CG7757	Prp3	v25548	9	6
FBgn0036487	CG6876	Prp31	v35131	3	2
FBgn0036487	CG6876	Prp31	v103721	6	3
FBgn0033688	CG6877	Prp8	v18565	12	7
FBgn0261552	CG42670	Ps	v44710	18	9
FBgn0261552	CG42670	Ps	v24214	10	5
FBgn0014870	CG8912	Psi	v28989	16	8
FBgn0014870	CG8912	Psi	v28990	10	5
FBgn0014870	CG8912	Psi	v105135	10	7
FBgn0028577	CG12085	pUf68	v109796	8	4
FBgn0003165	CG9755	pum	36676	12	7
FBgn0022987	CG4816	qkr54B	34896	10	5
FBgn0022986	CG3613	qkr58E-1	55159	10	5
FBgn0022985	CG5821	qkr58E-2	55279/CyOtb	6	3
FBgn0022984	CG3584	qkr58E-3	55922	10	5
FBgn0260944	CG17136	Rbp1	v21083/TM6B	12	6
FBgn0260944	CG17136	Rbp1	v110008	11	6
FBgn0030479	CG1987	Rbp1-like	v105883	10	6
FBgn0030479	CG1987	Rbp1-like	44100	4	2
FBgn0260943	CG32169	rbp6	61324/CyOtb	8	4
FBgn0015778	CG9412	rn	33392/TM6B	12	7
FBgn0003261	CG10279	Rm62	v46908/TM6B	12	6
FBgn0037707	CG16788	RnpS1	56910	10	5
FBgn0037707	CG16788	RnpS1	36580	6	3
FBgn0005649	CG5422	Rox8	v100563	10	5
FBgn0005649	CG5422	Rox8	v41439	12	6
FBgn0011305	CG5655	Rsf1	v22186/TM3	15	10
FBgn0267790	CG9373	rump	42665/CyOtb	6	3
FBgn0039229	CG6995	Saf-B	51759		5
FBgn0265298	CG5442	SC35	v40590	5	3
FBgn0265298	CG5442	SC35	v104978	6	3
FBgn0025571	CG5836	SF1	v13426	3	2
FBgn0040284	CG6987	SF2	v27775/TM3	13	7
FBgn0040284	CG6987	SF2	v27776/TM6B	6	4
FBgn0052423	CG32423	shep	43545	4	3
FBgn0002354	CG1420	Slu7	v103587	5	3
FBgn0262601	CG5352	SmB	v40587	3	2
FBgn0262601	CG5352	SmB	v110713	12	6
FBgn0261933	CG10753	SmD1	v31343/TM6B	8	4
FBgn0261933	CG10753	SmD1	v31342	7	4
FBgn0261789	CG1249	SmD2	v31947	4	2
FBgn0261789	CG1249	SmD2	v31946	8	4
FBgn0261789	CG1249	SmD2	v100690	4	2
FBgn0023167	CG8427	SmD3	v35933	8	5
FBgn0261790	CG18591	SmE	v23569	4	2
FBgn0261790	CG18591	SmE	v23570/TM6B	10	5
FBgn0000426	CG16792	SmF	v107644/CyOtb	lethal	
FBgn0000426	CG16792	SmF	26734	12	6
FBgn0036641	CG16725	Smn	v100392	7	4
FBgn0003449	CG4528	snf	51459	16	8
FBgn0003449	CG4528	snf	55914	9	5
FBgn0016978	CG8749	snRNP-U1-70K	v23150	11	8
FBgn0016978	CG8749	snRNP-U1-70K	v23151	10	6
FBgn0261792	CG5454	snRNP-U1-C	v22132	11	6
FBgn0261792	CG5454	snRNP-U1-C	v22133	10	5
FBgn0261791	CG9742	SNRPG	v39256	10	5
FBgn0015818	CG3780	Spx	v40471	9	5
FBgn0015818	CG3780	Spx	v40472	9	5
FBgn0263396	CG16901	sqd, hrp40	v32395	12	6
FBgn0263396	CG16901	sqd, hrp40	31302	20	10
FBgn0036340	CG11274	SRm160	v6439	9	5
FBgn0036340	CG11274	SRm160	v100751	8	4
FBgn0015298	CG4457	Srp19	51160	lethal	
FBgn0024285	CG4602	Srp54	v51088	8	6
FBgn0024285	CG4602	Srp54	55254	9	5
FBgn0026370	CG8174	SRPK	v103416	9	6
FBgn0025702	CG11489	srpk79D	v47544	8	5
FBgn0025702	CG11489	srpk79D	v47545	10	5
FBgn0003520	CG5753	stau	31247	9	5
FBgn0003559	CG17170	su(f)	v110125	6	3
FBgn0003638	CG3019	su(wa)	v25597	12	9
FBgn0003638	CG3019	su(wa)	v104716	10	5
FBgn0264270	CG43770	Sxl	34393	10	5
FBgn0037371	CG2097	Sym	v33470	9	5
FBgn0038826	CG17838	syp	56972	10	5
FBgn0038826	CG17838	syp	v33012	15	9
FBgn0025790	CG10327	TBPH	v38377	7	4
FBgn0025790	CG10327	TBPH	v38379	10	5
FBgn0003741	CG16724	tra	v2560	12	6
FBgn0003742	CG10128	tra2	v8868	9	5
FBgn0039117	CG10210	tst	v38356	8	4
FBgn0039117	CG10210	tst	v108216	12	6
FBgn0033378	CG8781	tsu	55367	11	6
FBgn0033378	CG8781	tsu	28955	9	5
FBgn0033210	CG1406	U2A	v17358/TM6B	9	5
FBgn0033210	CG1406	U2A	v109815	11	6
FBgn0017457	CG3582	U2af38	v110075	9	5
FBgn0017457	CG3582	U2af38	29304	13	7
FBgn0005411	CG9998	U2af50	v24176	11	6
FBgn0005411	CG9998	U2af50	v24177	10	6
FBgn0036733	CG6322	U4-U6-60K	v34242	8	6
FBgn0036733	CG6322	U4-U6-60K	v110393	10	6
FBgn0030354	CG1559	Upf1	43144	12	7
FBgn0028554	CG10203	xl6	v31203	14	8
FBgn0028555	CG10204	xl6	v100226	11	7
FBgn0021895	CG18426	ytr	55704	4	2

Fly genotypes

R cell RNAi experiments (Figure 1)

1. *w; GMR-GFP, GMR-Gal4/CyO; Dscam2.10B-LexA, LexAop-myr-tdTomato/TM6B*
2. *w; GMR-GFP, GMR-Gal4/CyO; Dscam2.10A-LexA, LexAop-myr-tdTomato/TM6B*
3. *w, UAS-Dcr-2; GMR-GFP, GMR-Gal4/CyO; Dscam2.10A-LexA, LexAop-myr-tdTomato/TM6B*
4. *w, UAS-Dcr-2; GMR-GFP, GMR-Gal4/UAS-mCD8-RFP; Dscam2.10A-LexA, LexAop-myr-tdTomato/+*
5. *w, UAS-Dcr-2; GMR-GFP, GMR-Gal4/UAS-mbl-RNAi(v28732); Dscam2.10A-LexA, LexAop-myr-tdTomato/+*
6. *w, UAS-Dcr-2; GMR-GFP, GMR-Gal4/+; Dscam2.10A-LexA, LexAop-myr-tdTomato/UAS-mbl-RNAi(TRiP.JF03264)*

***mbl* whole animal experiments (Figure 1)**

1. *w; +; Dscam2.10B-LexA, LexAop-myr-tdTomato/TM6B*
2. *w; +; Dscam2.10A-LexA, LexAop-myr-tdTomato/TM6B*
3. *w; mbl^{e127}/CyO,GFP; Dscam2.10A-LexA, LexAop-myr-tdTomato/TM6B*
4. *w; $mbl^{MI00976}$/CyO,GFP; Dscam2.10A-LexA, LexAop-myr-tdTomato/TM6B*
5. *w; $mbl^{MI04093}$/CyO,GFP; Dscam2.10A-LexA, LexAop-myr-tdTomato/TM6B*
6. *w; mbl^{e127}/ $mbl^{MI00976}$; Dscam2.10A-LexA, LexAop-myr-tdTomato/+*
7. *w; $mbl^{MI04093}$/ $mbl^{MI00976}$; Dscam2.10A-LexA, LexAop-myr-tdTomato/+*

***mbl ey-FLP* MARCM experiments (Figure 2)**

1. *w, ey-FLP; FRT42D, Tub-Gal80/FRT42D; Dscam2.10A-LexA, LexAop-myr-tdTomato, Act5c-Gal4, UAS-mCD8-GFP/+*
2. *w, ey-FLP; FRT42D, Tub-Gal80/FRT42D, mbl^{e27}; Dscam2.10A-LexA, LexAop-myr-tdTomato, Act5c-Gal4, UAS-mCD8-GFP/+*
3. *w, ey-FLP; FRT42D, Tub-Gal80/FRT42D, mbl^{e127}; Dscam2.10A-LexA, LexAop-myr-tdTomato, Act5c-Gal4, UAS-mCD8-GFP/+*

***mbl* expression experiments (Figure 3)** 1. *w; UAS-mCD8-GFP/+; mbl^{NP0420}-Gal4/+*

2. *w; UAS-mCD8-GFP/+; $mbl^{MI00139}$-Gal4/+*
3. *w; Dac-FLP/+; elav-Gal4/ UAS>stop>myr::smGdP-V5-THS-UAS>stop>myr::smGdP-cMyc*
4. *w; Dac-FLP/+; mbl^{NP0420}-Gal4/ UAS>stop>myr::smGdP-V5-THS-UAS>stop>myr::smGdP-cMyc*
5. *w; Dac-FLP/+; $mbl^{MI00139}$-Gal4/ UAS>stop>myr::smGdP-V5-THS-UAS>stop>myr::smGdP-cMyc*
6. *w; Dac-FLP/+; Dscam2.10A-Gal4/ UAS>stop>myr::smGdP-V5-THS-UAS>stop>myr::smGdP-cMyc*
7. *w; Dac-FLP/+; Dscam2.10B-Gal4/ UAS>stop>myr::smGdP-V5-THS-UAS>stop>myr::smGdP-cMyc*
8. *w; +; mbl^{NP0420}-Gal4/UAS-GFP.nls*
9. *w; +; $mbl^{MI00139}$-Gal4/UAS-GFP.nls*

***mbl* ectopic expression in MBs (Figure 4)**

1. *w; +; Dscam2.10A-LexA, LexAop-myr-tdTomato, Act5c-Gal4, UAS-mCD8-GFP/+*
2. *w; +; Dscam2.10B-LexA, LexAop-myr-tdTomato, Act5c-Gal4, UAS-mCD8-GFP/+*
3. *w; P{EP}mbl^{B2-E1}/+; Dscam2.10B-LexA, LexAop-myr-tdTomato, Act5c-Gal4, UAS-mCD8-GFP/+*
4. *w; +; Dscam2.10B-LexA, LexAop-myr-tdTomato, Act5c-Gal4, UAS-mCD8-GFP/UAS-mblA*
5. *w; +; Dscam2.10B-LexA, LexAop-myr-tdTomato, Act5c-Gal4, UAS-mCD8-GFP/UAS-mblB*
6. *w; +; Dscam2.10B-LexA, LexAop-myr-tdTomato, Act5c-Gal4, UAS-mCD8-GFP/UAS-mblC*
7. *w; +; Dscam2.10B-LexA, LexAop-myr-tdTomato, Act5c-Gal4,UAS-mCD8-GFP/UAS-$MBNL1_{35}$*
8. *w; +; Dscam2.10B-LexA, LexAop-myr-tdTomato, UAS-mCD8-GFP/UAS-mblA; OK107-Gal4/+*
9. *w; +; Dscam2.10B-LexA, LexAop-myr-tdTomato, UAS-mCD8-GFP/UAS-mblB; OK107-Gal4/+*
10. *w; +; Dscam2.10B-LexA, LexAop-myr-tdTomato, UAS-mCD8-GFP/UAS-mblC; OK107-Gal4/+*
11. *w; +; Dscam2.10B-LexA, LexAop-myr-tdTomato, UAS-mCD8-GFP/UAS-$MBNL1_{35}$; OK107-Gal4/+*

Lamina neuron FlpOut *mbl* LOF (Figure 5)

1. *w, 27G05-FLP/(+ or Y); Bl/CyO; Dscam2.10B-Gal4/ UAS>stop>myr::smGdP-V5-THS-UAS>stop>myr::smGdP-cMyc*
2. *w, 27G05-FLP/(+ or Y); Bl/CyO; Dscam2.10A-Gal4/ UAS>stop>myr::smGdP-V5-THS-UAS>stop>myr::smGdP-cMyc*
3. *w, 27G05-FLP/(+ or Y); mbl^{e127}/ CyO; Dscam2.10A-Gal4/ UAS>stop>myr::smGdP-V5-THS-UAS>stop>myr::smGdP-cMyc*
4. *w, 27G05-FLP/(+ or Y); $mbl^{MI00976}$/CyO; Dscam2.10A-Gal4/ UAS>stop>myr::smGdP-V5-THS-UAS>stop>myr::smGdP-cMyc*
5. *w, 27G05-FLP/(+ or Y); mbl^{e127}/ $mbl^{MI00976}$; Dscam2.10A-Gal4/ UAS>stop>myr::smGdP-V5-THS-UAS>stop>myr::smGdP-cMyc*
6. *w, 27G05-FLP/(+ or Y); elav-Gal4/LexAop2>stop>myr::smGdP-V5; Dscam2.10A-LexA/TM2*
7. *w, 27G05-FLP/(+ or Y); elav-Gal4/LexAop2>stop>myr::smGdP-V5; Dscam2.10B-LexA/TM2*
8. *w, 27G05-FLP/(+ or Y); elav-Gal4/LexAop2>stop>myr::smGdP-V5; Dscam2.10B-LexA/UAS-mblB*

L1 axonal and dendritic defects (Figure 5)

1. *w, 27G05-FLP/(+ or Y); Bl.CyO; Dscam2.10A-Gal4/ UAS>stop>myr::smGdP-V5-THS-UAS>stop>myr::smGdP-cMyc*

2. *w, 27G05-FLP/(+ or Y); mbl^{e127}/ mbl^{MI00976}; Dscam2.10A-Gal4/ UAS>stop>myr::smGdP-V5-THS-UAS>stop>myr::smGdP-cMyc*

***mbl ey-FLP* mosaic experiments (Figure S1)**

1. *w, ey-FLP; FRT42D, GMR-myr-GFP/FRT42D; Dscam2.10B-LexA, LexAop-myr-tdTomato, UAS-mCD8-GFP/+*
2. *w, ey-FLP; FRT42D, GMR-myr-GFP/FRT42D; Dscam2.10A-LexA, LexAop-myr-tdTomato, UAS-mCD8-GFP/+*
3. *w, ey-FLP; FRT42D, GMR-myr-GFP/FRT42D, Df(2R)154 ; Dscam2.10A-LexA, LexAop-myr-tdTomato, UAS-mCD8-GFP/+*
4. *w, ey-FLP; FRT42D, GMR-myr-GFP/FRT42D, mbl^{e27}; Dscam2.10A-LexA, LexAop-myr-tdTomato, UAS-mCD8-GFP/+*
5. *w, ey-FLP; FRT42D, GMR-myr-GFP/FRT42D, mbl^{MI00976}; Dscam2.10A-LexA, LexAop-myr-tdTomato, UAS-mCD8-GFP/+*

***mbl* expression (Figure S3)**

1. *w; mbl^{K01212}-LacZ*
2. *w; mbl^{NP1161}-Gal4/CyO, UAS-LacZ*
3. *w; mbl^{MI00139}-Gal4/+; UAS-CD8-GFP/+*
4. *w; mbl^{MI00139}-Gal4/UAS-GFP.nls*
5. *w; mbl^{NP0420}-Gal4/UAS-GFP.nls*

MB axon defects (Figure S5)

1. *w; +; +*
2. *w; +; Dscam2^{null}/ Dscam2^{null}*
3. *w; +; Dscam2A/ Dscam2A*
4. *w; +; Dscam2B/ Dscam2B*
5. *w; mbl^{e127}/ mbl^{MI00976}*
6. *w; +; +; OK107-Gal4/+*
7. *w; UAS-mbl-RNAi(v28732)/+*
8. *w; UAS-mbl-RNAi(v28732)/+; +; OK107-Gal4/+*
9. *w; PEPmbl^{B2-E1}/+*
10. *w; PEPmbl^{B2-E1}/+; +; OK107-Gal4/+*
11. *w; +; UAS-mblA/+*
12. *w; +; UAS-mblA/+; OK107-Gal4/+*
13. *w; +; UAS-mblB/+*
14. *w; +; UAS-mblB/+; OK107-Gal4/+*
15. *w; +; UAS-mblC/+*
16. *w; +; UAS-mblC/+; OK107-Gal4/+*
17. *w; +; UAS-MBNL1$_{35}$/+*
18. *w; +; UAS-MBNL1$_{35}$/+; OK107-Gal4/+*